aerospace

MDPI

Review

Serrations as a Passive Solution for Turbomachinery Noise Reduction

Andrei-George Totu [1,2], Grigore Cican [1,2,*] and Daniel-Eugeniu Crunțeanu [1]

[1] "Elie Carafoli" Department of Aerospace Science, Polizu Campus, National University of Science and Technology POLITEHNICA Bucharest, Splaiul Independenței 313, 060042 Bucharest, Romania; andrei.totu@comoti.ro (A.-G.T.); daniel.crunteanu@upb.ro (D.-E.C.)

[2] Romanian Research & Development Institute for Gas Turbines COMOTI, Iuliu Maniu Ave. 220D, 061136 Bucharest, Romania

* Correspondence: grigore.cican@upb.ro

Abstract: Aircraft engine noise has become a significant concern for air operators to address. Engineering strategies have resulted in the development of easily applicable solutions, known as "passive solutions", that do not necessitate real-time control. These solutions include the incorporation of corrugations or cutouts at critical locations on the engine's aerodynamic surfaces. Realistic solutions, whether approached numerically or tested at small scales, as well as computational models, have been found to closely match experimentally observed behaviors, both in 2D and 3D scenarios. The identified geometries serve as promising starting points for devising combined concepts that may offer even better performance under specific flow conditions.

Keywords: serrations; lowered noise emissions; fan noise; stator blade; interaction noise

check for updates

Citation: Totu, A.-G.; Cican, G.; Crunțeanu, D.-E. Serrations as a Passive Solution for Turbomachinery Noise Reduction. *Aerospace* **2024**, *11*, 292. https://doi.org/10.3390/aerospace11040292

Academic Editors: Weijie Chen and Weiyang Qiao

Received: 17 February 2024
Revised: 27 March 2024
Accepted: 7 April 2024
Published: 9 April 2024

1. Introduction

This paper aims to present the solution of utilizing modified blades in the leading and/or trailing edges to reduce noise generated by turbine engine rotor/stator blades. The proposed solution is passive, meaning it does not require additional installations to control specific blade parameters. Throughout the paper, the term "serrated vanes" or "serrated blades" will be used to refer to modified blades with repetitive structures, typically in the form of teeth. The technical methods for implementing such serrations and the acoustic implications of this solution, including current–blade interaction noise and self-noise, will be discussed. Additionally, aerodynamic implications will be considered. Various approaches for integrating this solution, as identified in the literature, will be reviewed, including serrations applied at the leading edge, trailing edge, or both, utilizing different variation laws such as sinusoidal (with constant or variable amplitude, fixed or variable pitch), step-type, triangular, fractal, etc.

As cities become increasingly crowded, aircraft noise has emerged as a significant and pressing issue, particularly as airports are no longer located in remote areas. Alongside other sources of noise pollution, such as traffic noise, aircraft noise has garnered attention due to its adverse effects on communities. Among the primary sources of aircraft noise are the propulsion systems, which include engines and related components. Engine manufacturers tend to further optimize the propulsion system, which has led to the development of turbofan engines with a very high bypass so that specific fuel consumption is significantly reduced. Under these conditions, it is obvious that the secondary flow, which bears a substantial mass of air, is one of the main sources of noise. There is a correlation between noise source weightings, depending on the technological solution. For a low bypass ratio turbofan engine, the fan noise is at a similar level as the jet noise. For higher ratios, necessary to lower the specific consumption, the fan is the main source of radiation, the noise being directed towards the front with a certain dominant frequency (corresponding to the angular velocity of the fan, the so-called BPF). The frequency range of interest, in which it is desirable for the solution to provide the greatest noise reductions, is 0.5–3 BPF. These frequencies therefore correspond to several engine operating regimes (from "approach" to "take off") and include the harmonics with the highest contribution to source (fan) emissions.

The justification for researching such solutions also comes in light of the directives that are emerging at the European level on noise emissions, with the aim of ensuring a better living environment for all citizens (applicable within the European Union). In this respect, there are regulations or directives at the European level that are transposed/enacted in one form or another in national legislation. For example, European Comission directive [1] on the assessment and management of environmental noise, which is similar to [2]. Other forms of European noise laws issued some time ago can also be identified, such as:

- limitation of aircraft noise—EASA Regulations [3,4]
- operational restrictions in the area of communities around airports [5]
- regulation on the flight of subsonic aircraft [6]

2. Calculation Methods and Models for Serrated Vanes (Interaction Noise)

2.1. Classic Blade

With the advancement of bladed machines (specifically turboshaft engines), inquiries have emerged regarding the diverse characteristics and dependencies of flows in relation to measurable phenomena. One of the concerns that arose in the early 1950s was the determination of the acoustic spectrum due to aerodynamic effects. In this respect, there are a number of authors who have undertaken both theoretical and experimental approaches (Curle, Lighthill, Philips, Proudman, and, to a certain extent, by analogy, Stratton) [7]. The most remarkable works that form the basis for describing how aerodynamic noise is generated, different from that generated by the vibration of a solid placed in a medium, have been identified as those of Curle and Lighthill. Starting from Navier–Stokes relations and conservation of momentum in a form proposed by Reynolds, the exact equation of fluid motion (Equation (1)) was transformed into relation (2) by adding source terms (mass Q(x,t) per unit volume, introduced at a given moment of time at position x) [7,8].

$$\frac{\partial^2}{\partial t^2} - a_0^2 \nabla^2_{\rho} = \frac{\partial^2}{\partial x_i \partial x_j}\left(T_{ij}\right) \tag{1}$$

where $T_{ij} = \rho v i^{\vartheta} j^{+} p_{ij} - a_0^2 \rho \delta_{i_j}$, ρ is the density, p_{ij} is the pressure component of the stress tensor, a_0 is the speed of sound in the fluid medium, and v_i is the component of the velocity in the $x_i(i = 1, 2, 3)$ direction.

Starting from relation (2), Curle [7] tried to further develop Lighthill's theory [9] and focused on the differences between acoustic intensities generated by sources with different characteristics (dipoles vs. quadripoles). Through his analysis, he arrived at the same relationship derived by Lighthill for quadrupoles (also referred to as Lighthill's 11th law), as well as a comparable relationship for dipole-type sources [7].

$$\rho - \rho_0 = \frac{1}{4\pi a_0^2} \frac{\partial^2}{\partial x_i \partial x_j} \int v \frac{T_{ij}\left(y, t - \frac{|x-y|}{a_0}\right)}{|x-y|} dy \tag{2}$$

This similarity between the two types of sources is mentioned in relation (3). The relationship is useful to evaluate, at least quantitatively, the specific acoustic effects of different sources specific to certain applications. For example, for airfoils, the suction side represents a dipole-type source, and the fluctuating flow in the shear state ("shear layer") corresponds to a quadrupole-type acoustic source, as noted by Turner [8].

$$\frac{I_Q}{I_B} \sim \left(\frac{U_0}{a_0}\right)^2 \cdot f(R) \tag{3}$$

Building on Curle's work, Amiet [10] attempted to develop the general relationships explored in the 1950s and applied them to a simplified airfoil (flat plate). He also identified that the environment in which the airfoils are placed is not undisturbed but can be considered "frozen turbulence", whose parameters describing the fluctuating behavior are constant in the three directions of propagation (constant wave numbers). In this way, using various mathematical techniques, he was able to derive a law for the PSD (power spectral density) using a specific turbulence of the von Karman spectrum model, which can be further converted into a sound pressure level (e.g., relation (4)).

$$SPL_{1/3} = 10\lg\left[\frac{Ld}{z^2}M^5\frac{\overline{u^2}}{U^2}\frac{\hat{k}_x^3}{\left(1+\hat{k}_x^2\right)^{7/3}}\right] + 181.3 \tag{4}$$

Obviously, "complete" theories are based on simplifying assumptions. The same is true of Amiet's theory, which, when applied to blades that have an aerodynamic cross-section, requires correction. One such correction, for example, identified by Tian [11], is relation (5).

$$SPL\ [dB] = \frac{9}{50}\frac{\frac{e}{c}}{\left(\frac{e}{c}\right)_{ref}}\frac{f}{U}\frac{\left(\frac{\Lambda}{c}\right)_{ref}}{\frac{\Lambda}{c}} \tag{5}$$

2.2. Leading Edge Serrated Blades

The modification of the leading edge, as identified in the literature, is a naturally inspired process (adaptations from birds [12] or marine animals [13] can be identified here). When discussing the modification of the leading edge through the introduction of serrations, it is worth noting that their theoretical study began to emerge in the 1990s, as highlighted by Lyu [12]. The models that were the basis for the development of the theory of modified leading edge vanes were also those mentioned in the previous chapter, namely Sears (1941), Curle (1955), Graham (1970), and Amiet (1972–1975). Lyu [12] built on these mathematical models and developed a theoretical methodology for characterizing the acoustic performance of such modified leading-edge vanes. He used various mathematical procedures, including Fourier series developments and Schwarzchild techniques, and finally identified that the main noise reduction occurs due to destructive interference induced by the pressure field strongly influenced by the presence of these modifications.

Lyu [12] identified that for a "uniform" flow, the non-stationarity of the velocity in the upstream region with respect to the analyzed blade can be decomposed according to several models: vorticity (a pseudo-velocity field), entropy, or acoustic waves. Typically, the non-stationarity of the upstream flow is assessed by a velocity field, which Amiet [10] also characterizes by a parameter w(x, y, t).

V. Clair et al. [14] attempted to validate the usefulness of such vanes using an internal solver. In order to get as close as possible to the real case (turbulence from the rotor reaching the stator blade), the authors checked how the blade behaves both in longitudinal and lateral gusts (whose behavior is described by two non-zero wave numbers). The conclusion of the numerical analyses, after the code has been validated with models/data already existing in the literature, is that the NACA 65(12)-10 airfoil vane behaves well acoustically at different upstream conditions, and the spectrum of the modified vane is below that of the reference vane, which is also confirmed by the experiments performed.

Lau et al. [15] used numerical simulations to study how a turbulent jet interacts with a serrated leading edge (using a symmetric airfoil). They noted that the best results are obtained when turbulence parameters and vortex amplitude are conveniently coupled. The trend they observed is that as the ratio of the sera amplitude to the incident gust wavelength increases, so does the noise reduction. The reduction is considerable at ratios greater than 0.3, with "optimum" values in the range 1–1.5 for this ratio.

Narayanan et al. [16] analyzed both numerically and experimentally different combinations of serration parameters for airspeeds of 60 m/s (applied to flat plates). The observed trend is that the serration amplitude is the one that provides the noise reduction; there is no difference in trend between the flat plate and the real airfoil; and the spectra recorded experimentally show a noise reduction on a logarithmic trend with respect to the serration amplitude. Also, in a previous paper, Naraynan et al. [17] noted that the flat plate better captures the noise reduction mechanisms (the reduction is also more noticeable) compared to the 3D profile (10 dB vs. 4 dB).

From the perspective of Chaitanya et al. [18], the introduction of leading edge serrations is a good way to reduce the "efficiency" with which vorticity is transformed into acoustic radiation through interaction with the solid (inclined) surfacing. Thus, the acoustic sources distributed on the inclined surface of the leading-edge serrate vanes are lower in intensity than in the case of the reference (straight leading-edge) vane. Kim [19] identified that at low frequencies, the sources at the base of the serrate are dominant, and as we consider higher frequencies, the weighting starts to be similar. In this way, a combined serration (consisting of several amplitudes, either obtained by combining two waves or a random function) could lead, in some cases, to interesting results.

Biedermann et al. [20] tried to find a dependence between flow parameters and sound pressure level reduction starting from a usual configuration (stator vane airfoil: NACA 65(12)-10, Reynold numbers of order 10^5, sinusoidal serration with variable parameters, and incidence in the range 0–10°). As a result, a number of interdependence relations between different linear combinations of the main parameters are obtained. The method of obtaining these relationships is linear regression; an example illustrating their form is depicted in Figure 1.

Term	OASPL_{BL}, dB	OASPL_{Serr}, dB	$\Delta\mathrm{OASPL}$, dB
$z/H(L)$	$-1.142\mathrm{E}+01 \cdot z/H$	$-1.357\mathrm{E}+01 \cdot z/H$	$+4.658\mathrm{E}+00 \cdot z/H$
$z/H(Q)$	$-5.152\mathrm{E}+01 \cdot (z/H)^2$	$-5.638\mathrm{E}+00 \cdot (z/H)^2$	$-4.574\mathrm{E}+01 \cdot (z/H)^2$
$Re \cdot Tu$	$+6.323\mathrm{E}-07 \cdot Re \cdot Tu$	$+1.715\mathrm{E}-07 \cdot Re \cdot Tu$	$+4.608\mathrm{E}-07 \cdot Re \cdot Tu$
$Re \cdot A/C$	— —	$+2.327\mathrm{E}-05 \cdot Re \cdot A/C$	$-1.876\mathrm{E}-05 \cdot Re \cdot A/C$
$Re \cdot \lambda/C$	— —	$-2.221\mathrm{E}-05 \cdot Re \cdot \lambda/C$	$+1.709\mathrm{E}-05 \cdot Re \cdot \lambda/C$
$Re \cdot z/H$	$-8.150\mathrm{E}-06 \cdot Re \cdot z/H$	$+1.574\mathrm{E}-05 \cdot Re \cdot z/H$	$-2.389\mathrm{E}-05 \cdot Re \cdot z/H$
$Tu \cdot A/C$	— —	$-2.349\mathrm{E}+00 \cdot Tu \cdot A/C$	$+1.951\mathrm{E}+00 \cdot Tu \cdot A/C$
$Tu \cdot \lambda/C$	— —	$-4.268\mathrm{E}+00 \cdot Tu \cdot \lambda/C$	$+3.847\mathrm{E}+00 \cdot Tu \cdot \lambda/C$
$Tu \cdot z/H$	$+3.069\mathrm{E}+00 \cdot Tu \cdot z/H$	$+2.115\mathrm{E}+00 \cdot Tu \cdot z/H$	$+9.546\mathrm{E}-01 \cdot Tu \cdot z/H$

(**a**)

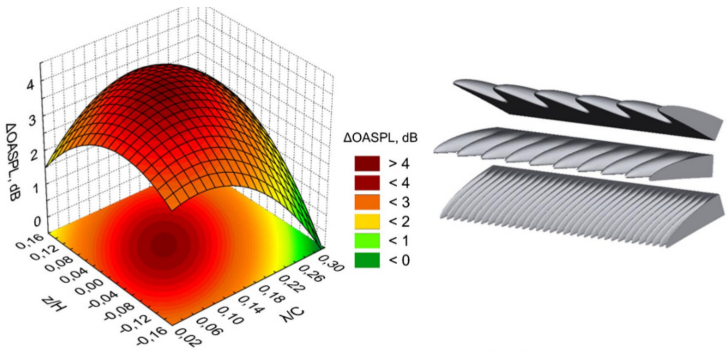

(**b**)

Figure 1. Example of interdependence between parameters (Biedermann [20]): (**a**) using linear regression; (**b**) plotting experimental data.

Although the relationships derived by Biedermann [20] are valuable, they only cover a limited range of operations, specifically regarding turbulence, chord, and associated serration parameters around certain values. A comprehensive characterization of such a vane requires a well-defined methodology, not solely reliant on experimental results. Naturally, the methodology must undergo validation through recordings conducted on dedicated stands; however, the material and time resources needed for this process should be significantly reduced. The most expedient approach capable of accommodating any combination of parameters is analytical or numerical calculation. In this regard, Lyu et al. [12] began with the models proposed by Amiet and analytically developed relations for determining the acoustic pressure and power field for a serrated blade with airflow over it. The starting point is the serrated flat plate illustrated in Figure 2 (which represents the simplest case).

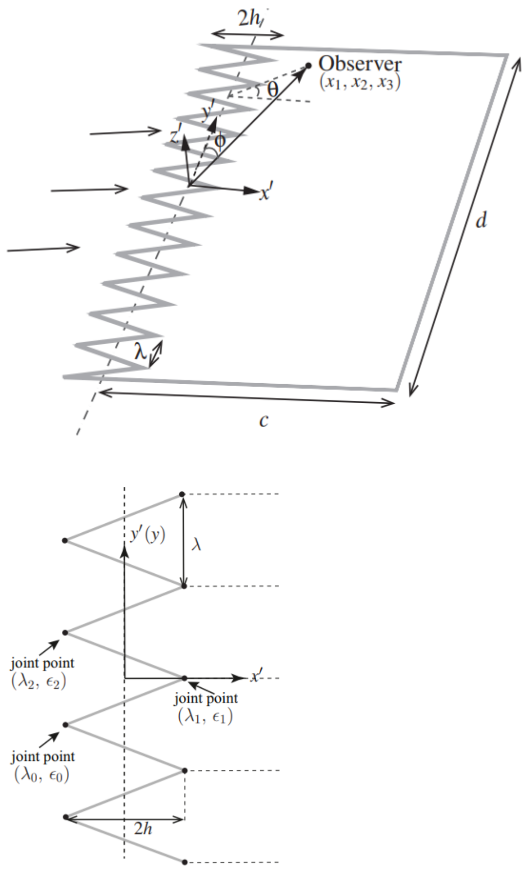

Figure 2. Schematic of a flat plate with triangular cut-outs in the leading edge area [12].

One can write a law describing the curve of the leading edge, and in this case, in triangular form, the variation law can be written according to relation (6):

$$H(y') = \begin{cases} \sigma_0(y' - \lambda_0 - m\lambda) + \varepsilon_0, & \lambda_0 + m\lambda < y' \leq \lambda_1 + m\lambda \\ \sigma_0(y' - \lambda_0 - m\lambda) + \varepsilon_1, & \lambda_1 + m\lambda < y' \leq \lambda_2 + m\lambda \end{cases} \tag{6}$$

where σ_j is the parameter defining how sharp the triangular serration is, λ_j is the distance in the span direction, and ε_j is the distance in the flow direction. The parameter m is an integer that can be either positive or negative (the origin of the system is placed at half the width/length of the blade) and defines the tooth number.

As previously mentioned, the turbulence associated with flow is considered isotropic and can be described by wave numbers associated with the propagation directions. Relation (7) presents a common formulation for turbulence coming from upstream to the serpentine leading edge.

$$w(x', y', t) = \int \int_{-\infty}^{\infty} \widetilde{w}(k_1, k_2) e^{i(k_1(x' - Ut) + k_2 y')} dk_1 dk_2 \tag{7}$$

This turbulence formulation can also be written in other forms, as presented by Lyu [12] or Amiet [10,21,22], with the calculation following a Fourier decomposition of the gust into simple plane waves of type (8).

$$w_i = w_{ia} e^{-i(\omega t - k_1 x' - k_2 y')} \tag{8}$$

The calculation is further based on solving a second-order differential equation for the potential velocity function, which is a wave propagation equation. Solving the equation using relation (8) leads to obtaining an equation system that has a matrix formulation of the type of relation (9), where A and B are two diagonal matrices, the problem being the wave-type system of PDEs that is solved iteratively.

$$D\Phi = A\Phi + B\frac{\partial \Phi}{\partial x} \tag{9}$$

where $\Phi = (\ldots \Phi_{-\mathrm{n}'}(x,z), \Phi_{-\mathrm{n}'+1}(x,z), \ldots \Phi_{\mathrm{n}'-1}(x,z), \Phi_{\mathrm{n}}(x,z), \ldots)^T$ and the matrices A and B are written as follows:

$$A_{ml} = \left(k_{2m}^2 - k^2\right)\delta_{ml},\ B_{ml} = \begin{cases} \frac{4\sigma}{\lambda}\frac{m+l+\frac{k_2\lambda}{\pi}}{l-m}, & m-l = even \\ 0\,, & m-l = odd \end{cases} \tag{10}$$

with δ_{ml} as the Kroneker symbol and m and l as the corresponding row and column index modes in the matrix, respectively.

The fundamental equation of the model developed by Lyu [12] is written in (11), where the sound pressure is written for the median plane of the vane.

$$S_{pp}(x,\omega) = (2\pi dU)\left(\frac{\rho_0 \omega x_3}{2\pi c_0 s_0^2}\right)^2 \sum_{m=-\infty}^{\infty} \frac{\Phi_{\omega\omega}(\omega|U, 2m\pi/\lambda)}{|\gamma_d(\omega|U, 2m\pi/\lambda)|^2}\left|\mathcal{L}\left(\omega, \frac{\omega}{U}, \frac{2m\pi}{\lambda}\right)\right|^2 \tag{11}$$

Note in relation (11) that the acoustic pressure depends on the spectrum of the incident turbulence (denoted here by $\Phi_{\omega\omega}$). There are several similar models, but the most common is the Von Karman spectrum, which in Amiet's formulation [10] is written according to (7). This spectrum can also be described using some experimentally recorded values (such as turbulence intensity and a parameter for length [23]). For three-dimensional flow with non-isotropic characteristics, Buszyk et al. [24] expressed the relationship for turbulence according to the three cartesian directions.

Lyu et al. [12] solved relation (11) for the experimental conditions used by Narayanan [16] and obtained the spectra in Figure 3, which, after 1000 Hz, follow the experimental curves quite well. Being a theory developed from Amiet's relations, it was expected that in the low frequency band there would be differences in sound pressure.

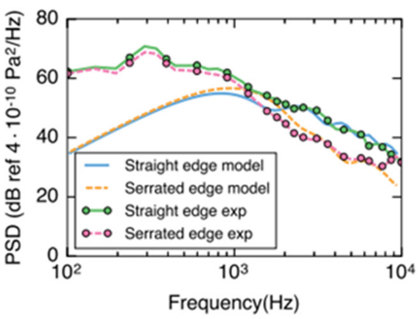

(a) $h/c = 0.067$.

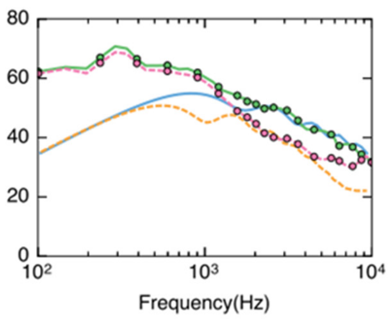

(b) $h/c = 0.167$.

Figure 3. Representation of results obtained with relation (10) versus experimental data [12].

As the calculation was performed in the median plane, we can say that it is a two-dimensional rather than a three-dimensional analysis so that, for isotropic turbulence, we could use the relation mentioned by Polacsek et al. [23] for the transition from the analyzed plane (2D) to a coordinate located anywhere in space (at a R_{obs} radius) using (12).

$$S_{pp}^{3D}(\omega) = S_{pp}^{2D}(\omega) \cdot \frac{k l_y(\omega) L}{2\pi R_{obs}} \tag{12}$$

where l_y is a correlation between the length of the vane, L, and the von Karman spectrum, and k is a parameter described in [23] as a combination of wave numbers, flow velocity, and serration angle.

2.3. Trailing Edge Serrated Blades

The trailing edge alteration that introduces serations was fully described for the first time in an analytical model by Howe [25]. It works similar to leading edge serations, with the notations being relatively the same. Howe started with the acoustic pressure relation in the far field written in integral form as a Fourier transform. From this, he rewrote it in the form of Green functions, which, after processing and correlation with the parameters of the serration, lead to a relation for the acoustic spectrum (relation (13)).

$$\begin{aligned} &\Psi(\omega) = \left(1 + \tfrac{1}{2}\epsilon \tfrac{\partial}{\partial \epsilon}\right) f\left(\tfrac{\omega\delta}{U_c}, \tfrac{h}{\lambda}, \tfrac{h}{\delta}; \epsilon\right), \\ &f\left(\tfrac{\omega\delta}{U_c}, \tfrac{h}{\lambda}, \tfrac{h}{\delta}; \epsilon\right) \\ &= \frac{1}{\left\{\left(\frac{\omega\delta}{U_c}\right)^2 \left[1 + \left(\frac{4h}{\lambda}\right)^2 + \epsilon^2\right]\right\}} \\ &\cdot \left(1 + \frac{64\left(\frac{h}{\lambda}\right)^3 \left(\frac{\delta}{h}\right)\left(\frac{\omega\delta}{U_c}\right)^2 \left\{cosh\left\{\frac{\lambda}{2\delta}\sqrt{\left[\left(\frac{\omega\delta}{U_c}\right)^2 + \epsilon^2\right]}\right\} - \cos\left(\frac{2\omega h}{U_c}\right)\right\}}{\sqrt{\left[\left(\frac{\omega\delta}{U_c}\right)^2 + \epsilon^2\right]}\left\{\left(\frac{\omega\delta}{U_c}\right)^2\left[1 + \left(\frac{4h}{\lambda}\right)^2\right] + \epsilon^2\right\} sinh\left\{\frac{\lambda}{2\delta}\sqrt{\left[\left(\frac{\omega\delta}{U_c}\right)^2 + \epsilon^2\right]}\right\}}\right) \end{aligned} \tag{13}$$

If in the previous relation (13) the serration amplitude (here h-semiamplitude) tends to 0, then the spectrum is obtained for the normal (straight) leading edge blade. Howe solved Equation (13) for several combinations of seration amplitudes and steps at a constant turbulent boundary layer amplitude/thickness ratio (Figure 4). The same equations were also solved by Al Tlua [26] in his PhD work using a code written in Matlab, obtaining identical results. He also made a comparison between the results obtained with a triangular greenhouse trailing edge vane versus a sinusoidal trailing edge, which he characterized in a similar way in a paper published in the same year.

For terms not described in this chapter related to relation (13), additional relations suggested by Moreau et al. [27] can be used where all experimental constants as well as relations corresponding to the turbulent boundary layer thickness (relations in (14)) are clarified.

$$\begin{gathered} \delta = 8\delta^* \\ \frac{\delta}{c} = \frac{0.37}{Re_c^{1/5}} \end{gathered} \tag{14}$$

Al Tlua [26] also identified a more complete relation (relation (15)), similar to the previous one, for the turbulent boundary layer thickness.

$$\delta = \frac{0.37c\left[1 + \left(\frac{Re_c}{6.9 \cdot 10^7}\right)^2\right]^{1/10}}{Re_c^{1/5}} \tag{15}$$

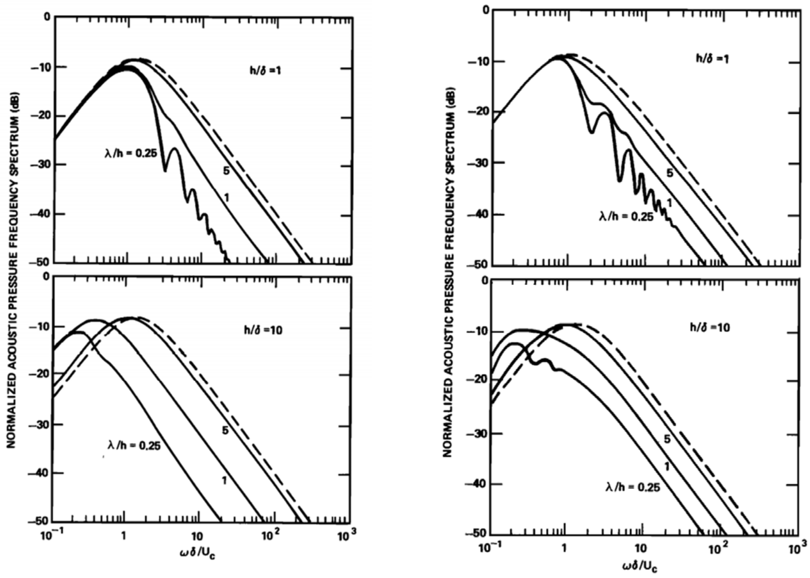

(**a**) (**b**)

Figure 4. Comparative analysis between spectra of trailing edge-modified vanes (dashed line- straight trailing edge) [25]: (**a**) triangular serrations; (**b**) sinusoidal serrations.

Lyu [28] solved the same problem of triangular serrations placed at the trailing edge and obtained a similar relationship to that of triangular serrations placed at the leading edge. The meaning of the terms in relation (16) is the same as those in relation (11), with the relations being quite close.

$$S_{pp}(x,\omega) = \left(\frac{\omega x_3 c}{4\pi c_0 s_0^2}\right)^2 2\pi d \sum_{m=-\infty}^{\infty} \left|\mathcal{L}\left(\omega, \frac{\omega}{U}, \frac{2m\pi}{\lambda}\right|^2 \Pi(\omega, 2m\pi/\lambda) \quad (16)$$

In Figure 5, Lyu et al. [28] conducted a comparative analysis between Howe's model (Equation (13)) and their own model (Equation (16)), identifying a relatively strong similarity between the two methods. From the two plots, it can be observed that the spectrum obtained with Howe's method [25] overestimated the noise reduction. Howe, at the time of publication, achieved a reduction of at least $10 \cdot \log[1 + (4h/\lambda)^2]$ dB, which could lead to values exceeding 10 dB under certain conditions. Over the years, several authors have shown that the reduction exists using such sera but is usually less than half of the values given by the mentioned relation.

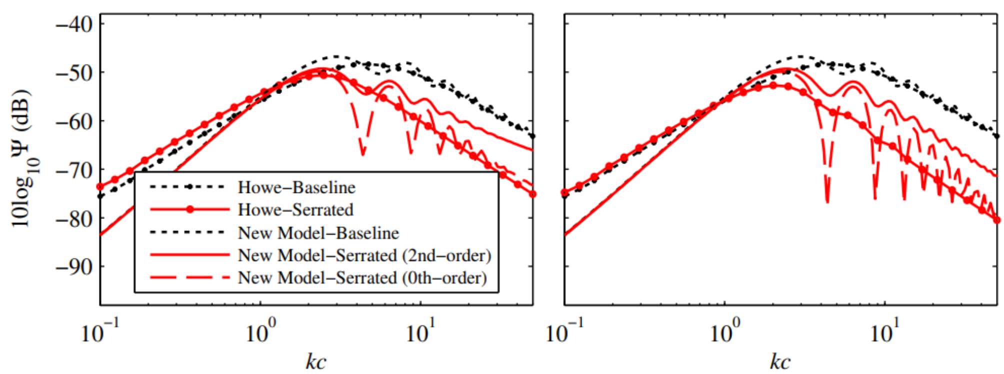

Figure 5. Comparison between the model proposed by Lyu et al. [28] and Howe [25] (**left**—λ/h = 0.4, h/c = 0.05, M = 0.1; **right**—λ/h = 0.2, h/c = 0.05, M = 0.1) [28].

Lau et al. [29] proposed a stepwise model for determining the acoustic spectrum generated by the change in the trailing edge. The first step is the definition of the gust parameters, calculated using two Fourier series development relations. The second step is to calculate the amplitudes of the n-th-order components using the Wiener-Hopf model. The third step is to combine the n components to obtain the spectrum. Using this method, the authors were able to characterize the behavior of triangular, sinusoidal, sawtooth, or slot-type trailing edges. Figure 6 shows the contours for the sound pressure level at M = 0.1.

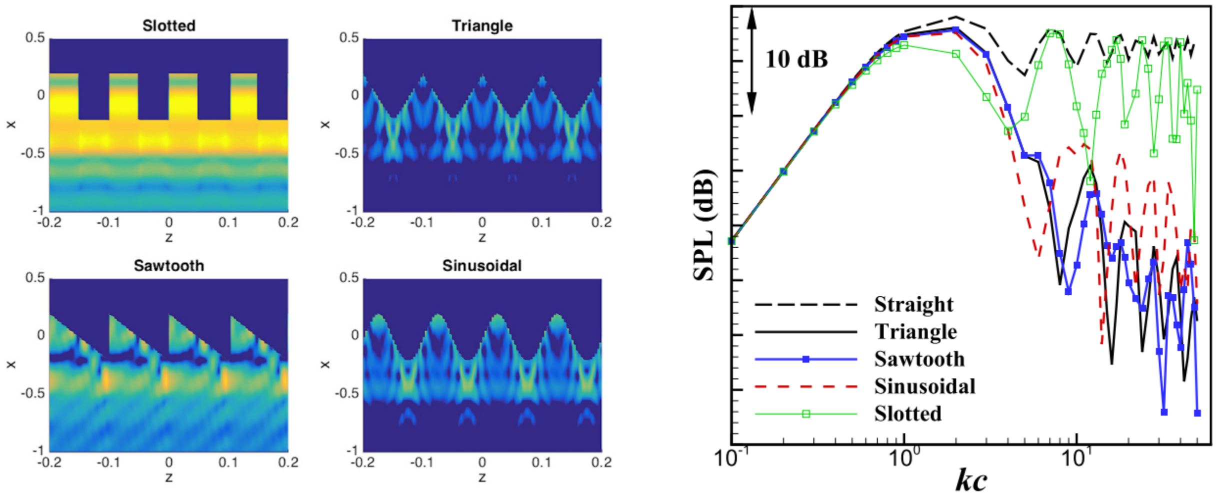

Figure 6. Comparison of sound pressure levels for different solutions applied to the trailing edge [29].

Woodhead et al. [30] applied triangular serrations to the trailing edge with a tilt of $\pm 15^\circ$ in order to observe significant changes in the acoustic spectrum. The downward (to the pressure side) inclined serrations did not provide an additional noise reduction effect, but on the contrary, over the whole frequency range, a lower attenuation was obtained compared to the initial version. When the serrations were placed in the other direction, the spectrum was modified in three areas, with the central area (mid-frequency) being positively impacted, which is due to secondary flows that modify the location of the acoustic sources. Similar trends were observed at higher frequencies. A more detailed analysis, also using the information obtained by Liu et al. [31] as well as Leon et al. [32], who measured velocity distributions using hot-wire instruments and visualized the flow near a triangular serration using specialized optical instruments, can be performed to obtain a better-performing geometry. Similarly, Chen et al. [33] tested and analyzed the results obtained for 12 different combinations of pure sera on the trailing edge.

Al Tlua [26] also analyzed the types of serrations mentioned by Lau [29], and as shown in Figure 6, he managed to identify the analytical relations for several variations: straight trailing edge (relation (17)), triangular trailing edge (relation (18)), slotted trailing edge (relation (19)), and sinusoidal trailing edge (relation (20)).

$$\Psi_{straight}(\omega) = \frac{\left(\frac{\omega\delta}{U_c}\right)^2}{\left[\frac{\omega\delta}{U_c} + \varepsilon^2\right]^2} \tag{17}$$

where convection velocity $U_c = 0.77U$ and empirical values $C_m = 0.1553$ and $\varepsilon = 1.33$.

$$\Psi_{\text{tri}}(\omega) = 8\left(\frac{h}{\delta}\right)^2\left(\frac{\omega h}{U_c}\right)\sum_{n=-\infty}^{\infty}\frac{\left[1 - cos\left(\frac{2\omega h}{U_c}\right)/cos(n\pi)\right]\left[\left(\frac{\omega h}{U_c}\right)^2 + \left(\frac{2n\pi h}{\lambda}\right)^2\right]}{\left[(n\pi)^2 - \left(\frac{2\omega h}{U_c}\right)^2\right]^2\left[\left(\frac{\omega h}{U_c}\right)^2 + \left(\frac{2n\pi h}{\lambda}\right)^2 + \left(\frac{\varepsilon h}{\delta}\right)^2\right]^2} \tag{18}$$

$$\Psi_{\text{slot}}(\omega) = \sum_{n=-\infty}^{\infty} \Theta\Theta^* \frac{\left[\left(\frac{\omega h}{U_c}\right)^2 + \left(\frac{2n\pi\delta}{\lambda_1+\lambda_2}\right)^2\right]}{\left[\left(\frac{\omega h}{U_c}\right)^2 + \left(\frac{2n\pi\delta}{\lambda_1+\lambda_2}\right)^2 + (\varepsilon^2)^2\right]^2} \tag{19}$$

where $\Theta(K, \lambda_1, \lambda_2, h) = n^{-1}\left[\left(e^{\frac{2in\pi\lambda_1}{\lambda_1+\lambda_2}} - 1\right)e^{iK_1 h} + \left(1 - e^{-\frac{2in\pi\lambda_1}{\lambda_1+\lambda_2}}\right)e^{-iK_1 h}\right]$.

$$\Psi_{sin}(\omega) = \left(\frac{\omega h}{U}\right) \sum_{n=-\infty}^{\infty} J_n^2\left(\frac{\omega h}{U}\right) \frac{\left(\frac{\omega\delta}{U}\right)^2 + \left(\frac{2n\pi\delta}{\lambda}\right)^2}{\left[\left(\frac{\omega\delta}{U}\right)^2 + \left(\frac{2n\pi\delta}{\lambda}\right)^2 + \varepsilon^2\right]^2} \tag{20}$$

Both with the above relations for the normalized spectra (from (17)–(20)) and with (11) and (16), a transformation as (20) should be made:

$$OASPL_{norm} = 10lg\left(\int_{\omega_{min}}^{\omega_{max}} \Psi(\omega)\, d\omega\right) \tag{21}$$

Ryi and Choi [34] also aimed to reduce noise by modifying the trailing edge, but their application focused on wind turbine rotor airfoils. They used an experimental wind tunnel setup placed in an anechoic chamber to characterize a constant chord (350 mm) and torsion-free wind turbine blade using six different types of greenhouses. The result of these experiments is an empirical law for the sound pressure level reduced by these methods. The model is composed of six relations (22)–(27), which are written as follows:

- expected acoustic spectrum

$$S(f) \approx \frac{1}{8\pi^2 R^2}\left(\frac{U_c L}{c_0}\right) l_u(f)\Phi(f) \tag{22}$$

- oscillatory function associated with the trailing edge

$$l_u(f) = \frac{U_c}{\xi 2\pi f} \tag{23}$$

- the term for solid surface pressure

$$\Phi(f) = \frac{\Phi(St^*) l q^2}{U_{max}} \tag{24}$$

- function for Strouhal number

$$St^* = \frac{f L(x)}{U_{max}} \tag{25}$$

- correlation of turbulence with lateral direction

$$L(x) = \left[log\left(\frac{\lambda_s}{h}\right)^{0.015} + 0.12\right] \tag{26}$$

- function for estimating noise reduction at the trailing edge

$$SPL_{serBF} = 3.5 - 8[\log(St^*) + 0.3]^2 - \left[\log\left(\frac{\lambda_s}{h}\right) + 0.4\right]^2 \tag{27}$$

2.4. Generating a Tonal Component

As Teruna et al. [35] noted, the rods are very good elements for generating the tonal component, especially in that they generate essentially the same fluctuation throughout their span/length (Figure 7).

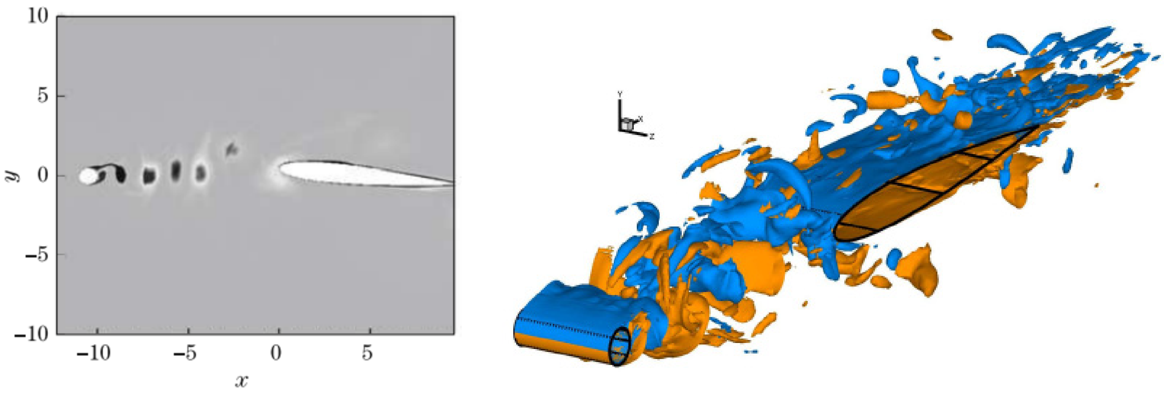

(**a**) (**b**)

Figure 7. Aerodynamic rod–profile interaction: (**a**) longitudinal plane view (2D) [36]; (**b**) visualization of turbulent structures as $\omega d/U = \pm 1$ (in blue/orange) (3D) [37].

The less favorable aspect is that in the case of an actual flow (inside a gas turbine), the turbulence generated by the rotor differs significantly from the behavior observed along the blade span. Sreenivasan [38] performed a series of numerical simulations to characterize the behavior of a rod placed in flow and used a series of turbulence models with which he obtained the Strouhal number associated with the phenomenon. Li [36] used even more detail and showed how the acoustic spectrum generated by the interaction between a rod and an airfoil is influenced as a function of flow incidence (Figure 8).

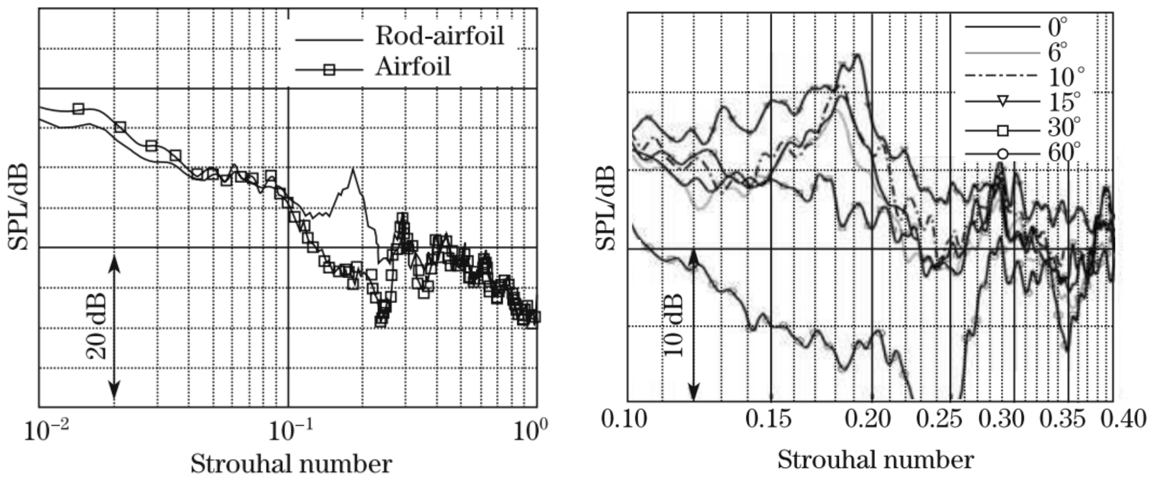

(**a**) (**b**)

Figure 8. Aerodynamic rod–profile interaction (M = 0.1) [36]: (**a**) 0 degree incidence with isolated profile and rod + profile; (**b**) rod + profile (positive AoA) at multiple degree incidences.

2.5. Generating Broadband Turbulence

In order to study the aeroacoustic behavior of the blades, a wind tunnel-type installation is often used, which must integrate an element that disturbs the flow from the fan so that it comes as close as possible to the operating conditions in the engine. In this respect, it is often preferred to use a "grid" conveniently placed on the test path (Figure 9) so that the flow takes on certain characteristics (to favor separation and reattachment at a certain frequency in certain directions). In the literature, it has been identified that most of the wind tunnel-type installations intended for the study of serrate vanes (either at the leading edge or the trailing edge) use such elements, which, over time, have been very well characterized.

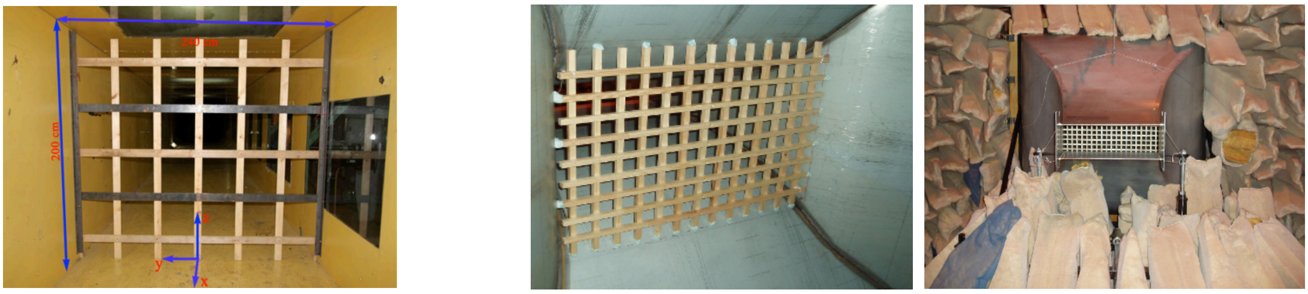

(**a**) (**b**)

Figure 9. Placing a turbulence grid on the test section: (**a**) the wind tunnel at Southwest Jiao-Tong University [39]; (**b**) the ISVR wind tunnel [40].

Liu et al. [39] attempted to characterize the behavior of several grids integrated into their experimental setup using numerical analysis. Gruber [40] used both experimental and theoretical methods, including the von Karman model [12] as a reference (relation (28)). A similar approach was taken by Chaitanya [41], who experimented at several incident flow speeds (Figure 10). This relation has also been identified with other notations in several papers (Biedermann [20] and Polacsek [23]).

$$\Phi_{ww}(k_1, k_2) = \frac{4\overline{u^2}}{9\pi k_e^2} \frac{\hat{k_1}^2 + \hat{k_2}^2}{\left(1 + \hat{k_1}^2 + \hat{k_2}^2\right)^{7/3}} \tag{28}$$

where $k_e = \frac{\sqrt{\pi}\Gamma(5/6)}{L_t\Gamma(1/3)}$, $\hat{k_1} = \frac{k_1}{k_e}$, and $\hat{k_2} = \frac{k_2}{k_e}$.

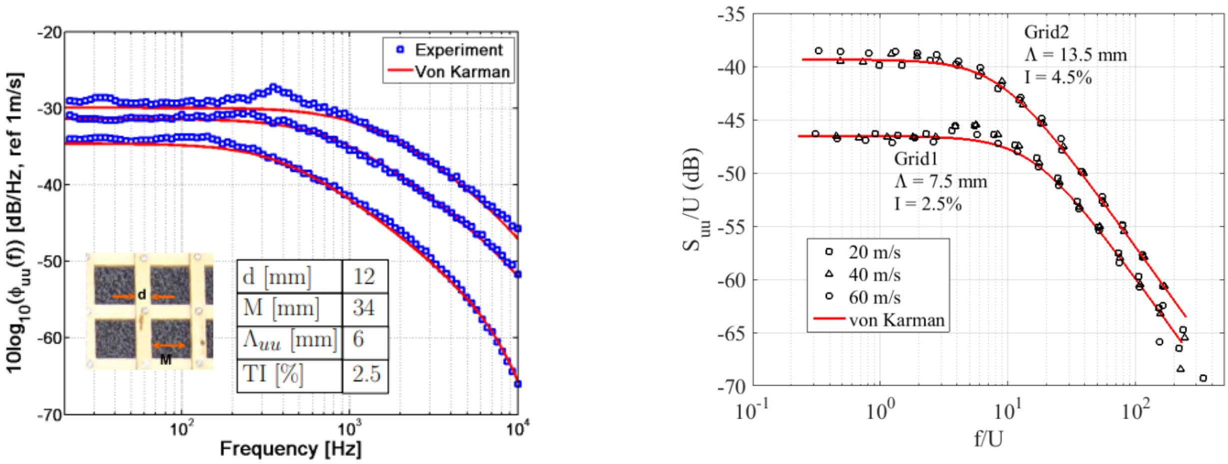

(**a**) (**b**)

Figure 10. Von Karman spectrum: (**a**) extract from Gruber [40]; (**b**) extract from Chaytania [41].

The spectrum of dimensionless turbulence, denoted by Lyu et al. [42] with $\Pi_1(\omega,k_2)$, can be characterized using the Liepmann model, which is written according to relation (29). Similar to the von Karman spectrum, the formulations are similar, with the notations being slightly adapted from author to author (Amiet [10,22], Biedermann [20], and Chaytania [43]).

$$\Pi_l(\omega, k_2) = \frac{3TI^2L_t^2}{4\pi} \frac{L_t^2\,(k_1^2 + k_2^2)}{\left(1 + L_t^2\,(k_1^2 + k_2^2)\right)^{5/2}} \tag{29}$$

where TI and Lt represent the turbulence intensity and the integral lenth scale, respectively, parameters that are often determined experimentally. An equation with a slightly simpler formulation (including an exponential) is used by Al-Okbi [44]. In Figure 11, Biedermann [20] performs a characterization of a turbulence grid using Liepmann's formulation.

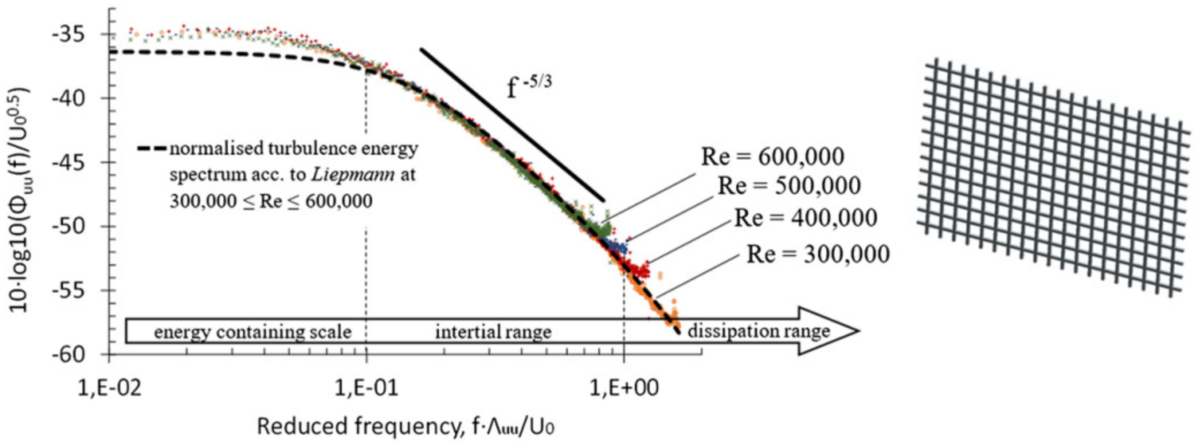

Figure 11. Representation of the recorded spectrum for a turbulence grid at different Re numbers (highlighted in different colors) [20].

As can be seen from Figures 10 and 11, the theoretically obtained spectra are similar using both models. Amiet [22] showed that in the axial direction, the two models are almost identical, although there are small differences in the vertical component (Figure 12, 2D coordinates).

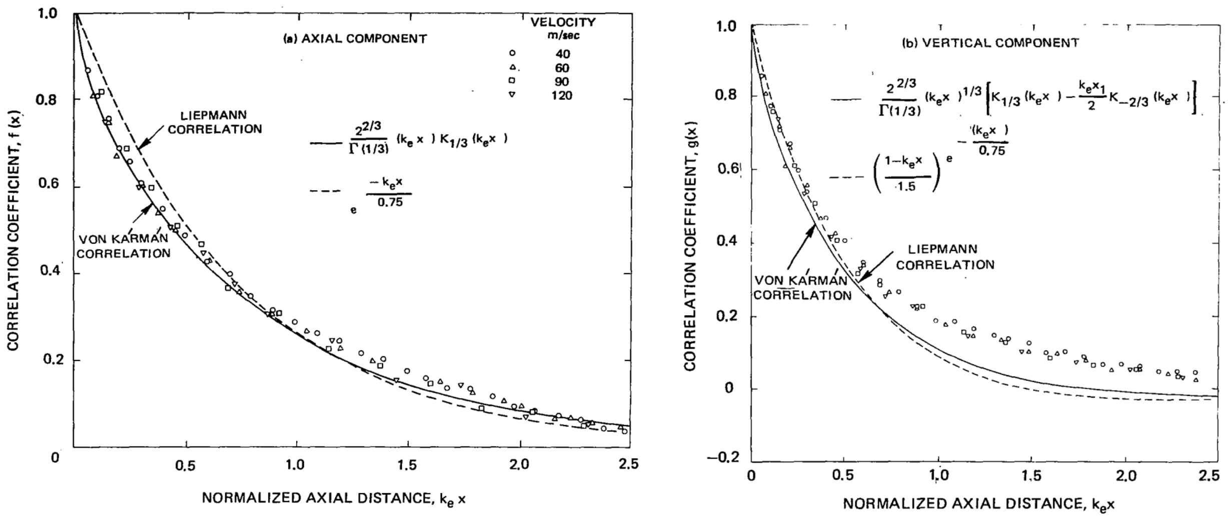

Figure 12. Comparative analysis between axial and vertical components for von Karman and Liepmann models [22].

3. Aerodynamic Considerations

Tong et al. [45] numerically investigated a stator airfoil, NACA 65(12)-10, both acoustically and aerodynamically. After post-processing, the authors observed that the used serration behaves as a delta wing, with two areas of significant vorticity in the lateral direction affecting flow in the longitudinal direction when the serration is placed at the leading edge (Figure 13). Since a rod (which generates a tonal component) has been placed in front of the blade, it can be observed that the noise reductions are semi-effective (11–16 dB for a fairly large range of the St parameter).

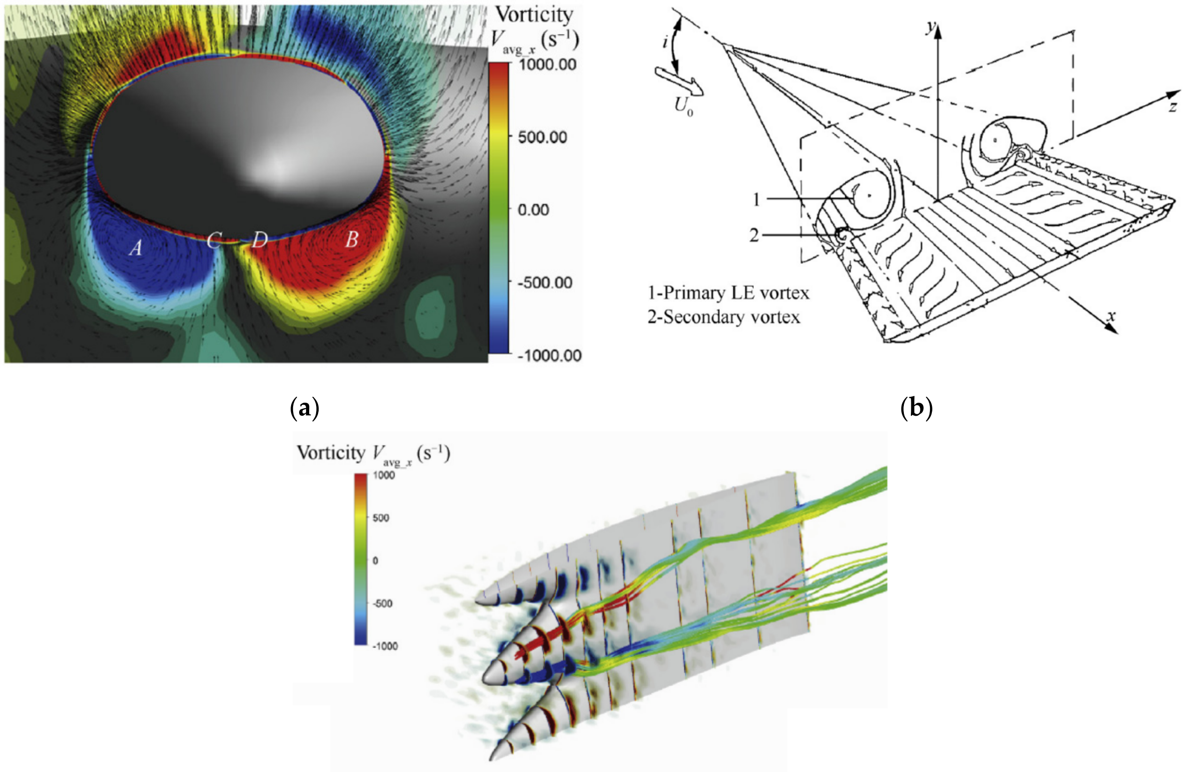

(**a**) (**b**)

(**c**)

Figure 13. Aerodynamic effects as a result of placing serration on the leading edge [45]: (**a**) peak region; (**b**) lateral vortices; (**c**) streamlines-tooth downstream.

As interesting as the acoustic values are, so are those related to aerodynamic performances. Figure 14 shows a comparison of the variations in the lift (C_L) and drag (C_D) coefficients for the reference (straight leading edge) and serrated (sinusoidal leading edge) vanes. It is observed that, although in mean values the coefficients do not have very large variations, in RMS values the behavior of the blade changes quite a lot. The author [45] observed that, although the flow changes its character, the variation in forces on the aerodynamic surface becomes more stable following the use of such a leading edge.

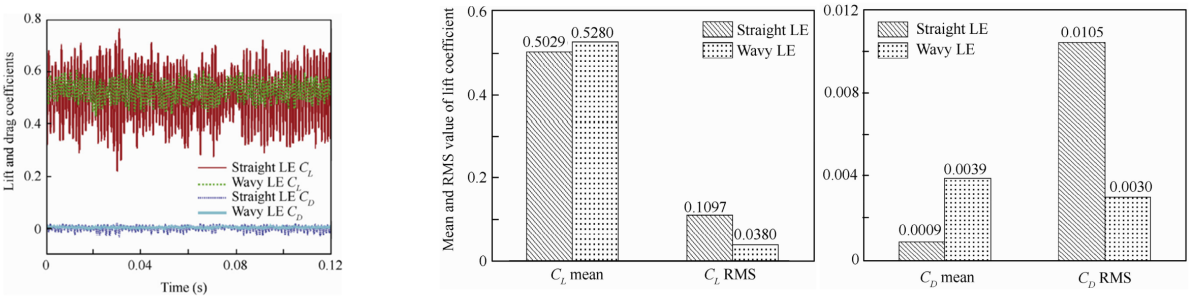

(**a**) (**b**)

Figure 14. Aerodynamic behavior for a serrated blade placed in a flow [45]: (**a**) aerodynamic coefficients—time variation; (**b**) histograms for aerodynamic coefficients.

Teruna et al. [35] used aeroacoustic (LBM) simulations to characterize the behavior of vanes with both symmetric NACA and curved NACA profiles. For the treatment of the leading edge, various solutions are chosen, either simple serrations, porous serrations, geometrically unmodified but porous leading edges, or combinations thereof. Porous variants (where a Ni-Cr-Al sponge was used) facilitate the appearance of lateral curvature, so that aerodynamic performance is also reduced. Also, by modifying an important area of the leading edge for the integration of the solution, in the case of the porous material, communication between the suction and pressure sides is possible, which leads to additional undesired flows. Figure 15 shows the aerodynamic implications of using the serrations in the simple version or with integrated porous material.

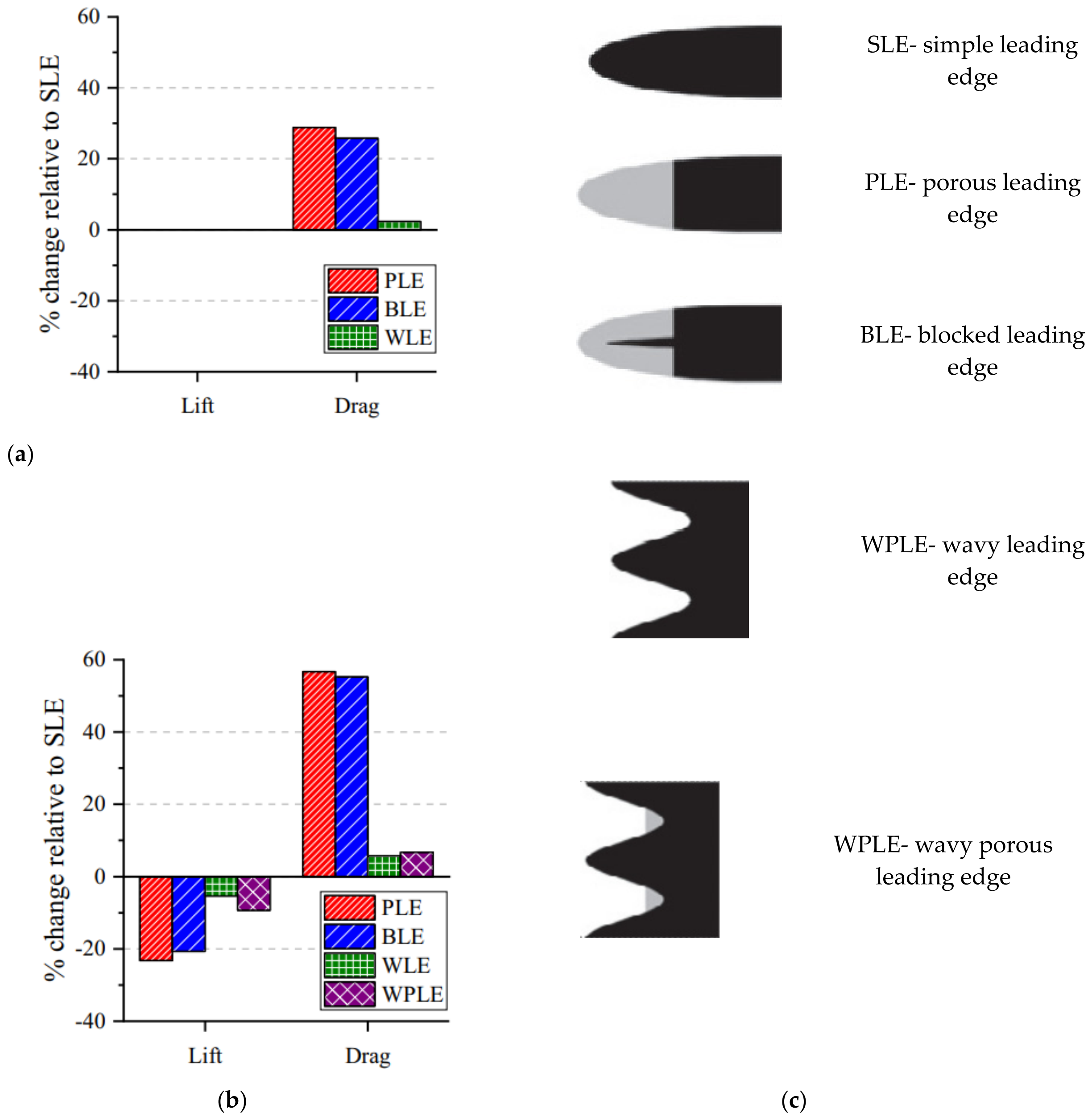

Figure 15. Influence of porous and/or serated leading edge on aerodynamic performance (extracted from [35]): (**a**) NACA0012; (**b**) NACA5406; (**c**) leading edge geometries.

Ito [46] also investigated the behavior of a stator blade (NACA63-414 airfoil), to which he applied a serrated region (sawtooth type) with a small amplitude (approximately 1% of the chord length, which was 152 mm) at the leading edge. The aim was to identify how aerodynamic performance is affected or enhanced at low Reynolds numbers (on the order of 104–105). Using a wind tunnel setup, the 250-mm-long blade was positioned between two plates (to minimize end-of-plane losses) and connected to a three-component load cell force transducer. The same setup was used for flow visualization. Although no changes in the values of lift coefficients or inlet resistance were detected, the author noted that the serrations delayed flow detachment on the suction side of the upper surface (in the initial phase) and promoted the formation of a vortex at high angles of attack, which tended to adhere the fluid to the solid surface. This phenomenon was observed at both low and high speeds, albeit with lower efficiency at higher Reynolds numbers. The number of teeth used ranged from 16 to 28 per inch, and denser arrangements exhibited superior aerodynamic behavior, as confirmed by force measurements and smoke visualization. Figure 16 illustrates the lift and drag coefficients for the case of a low Reynolds number (2.1 $\times$ 10^4). No significant differences were observed for higher Reynolds numbers (2.1 $\times$ 10^5).

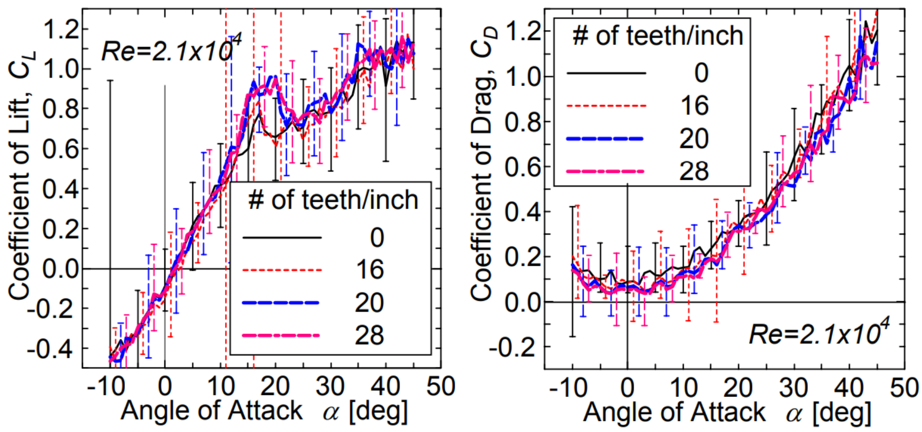

Figure 16. Comparison between a straight leading edge vane and a tooth-serrated vane [46].

In an attempt to validate an in-house code for numerical analysis of modified leading edge blades, Polacsek [23] presented some interesting data, also validated by experiments performed by his team over time. Among these interesting data was the distribution of pressure coefficients in different areas of a serration (top, middle, and bottom), which obviously correspond to atypical pressure distributions, especially in the leading edge area (the low pressure area at the stagnation point "joins" the low pressure area at the trailing edge in the LE part). In Figure 17, the distribution of pressure coefficients as well as the distribution of pressures in a logitudinal section (along the flow) can be observed.

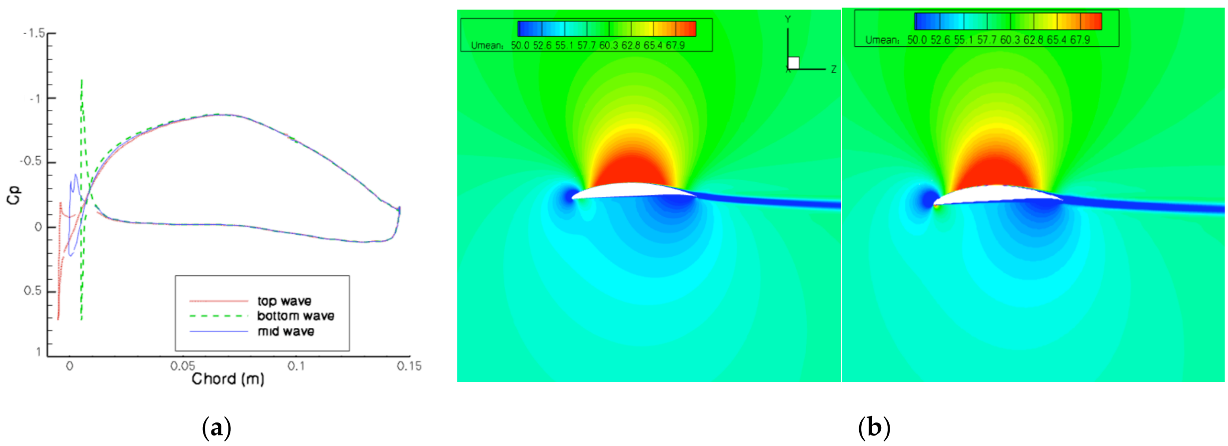

Figure 17. Pressure distribution on a vane with a wavy leading edge [23]: (**a**) Cp distribution; (**b**) pressure distribution at the top of the serration (**left**) and in the middle of the serration (**right**).

4. Configurations of Interest Identified in the Literature

Throughout the paper, various sources have been mentioned that present a multitude of blade variants. The simplest geometry is the flat plate placed in flow, for which the theoretical solution to obtaining the pressure and velocity field has been obtained analytically since the 1950s. It has been validated by several authors over time and adapted so that it can be compared with more complex models associated with serrated vanes. The theoretical development (from an analytical point of view) of blades with a serrated leading edge or trailing edge was carried out starting from the flat plate model, to which the law of variation in the areas of interest was modified. Important contributions have also been identified experimentally, with several authors obtaining either empirical/semi-empirical laws that link the incident current turbulence parameters with the serration parameters so as to obtain an optimal noise reduction. Table 1 summarizes some of the relevant geometries, analyzed over time, together with some test conditions required for a comparative analysis (two- or three-dimensional solution, broadband turbulence given by a grid, or tonal component given by a rod placed upstream).

Table 1. Modified blades on the leading edge.

Crt. No.	Serration Shape	Author, Year	Solution Type		Type of Turbulence		Results	Observations
			2D	3D	Grid	Rod		
1	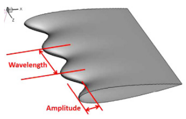 Sinusoidal [15]	Lau et al. [15], 2013		☒	-	-	LEA/λ ≈ 1 for maximum noise reduction (minimum LEA/λ > 3)	Simulation, no grid, upstream pressure fluctuations model
2	Triangular flat plate	Lyu et al. [12], 2017	☒		☒		ωh/U >> 1 for significant noise reductions	Analytic model
3	Complex sinusoidal 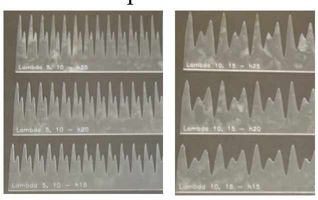 [18]	Chaitanya et al. [18], 2016	☒		☒		h_{tt}/λ = 1 optimum (as a result of interferences)	experimental Umax ~ 80 m/s
4	Complex sinusoidal 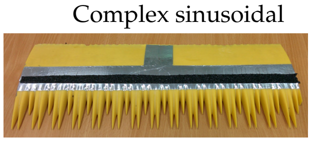 [18]			☒			Weak aerodynamic performances at low AoA	
5	Triangular cut-outs 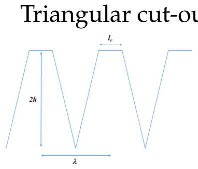 [18]		☒				High l_c/λ for low freq. performances (l_c-cutout width)	
6	Triangular serration with slots 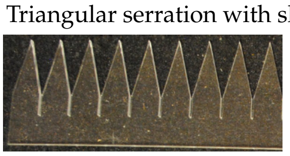 [18]		☒				Optimum width– pitch ratio (here w/λ = 0.13)	

Table 1. *Cont.*

Crt. No.	Serration Shape	Author, Year	Solution Type		Type of Turbulence		Results	Observations
			2D	3D	Grid	Rod		
7	Triangular serration with slots 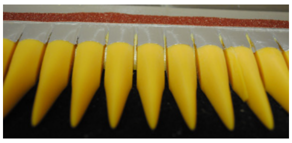 [18]			☒			As good as 2D at fh/U > 0.8; low performances for fh/U > 0.8	
8	Double triangular slots 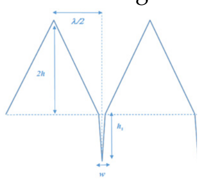 [18]		☒				Better with higher slot height; optimum reached as for straight slot	
9	Sinusoidal  [41]	Chaitanya et al. [41], 2017		☒	☒		Max. acoustic performance for $\lambda/\Lambda_t \approx 4$; acoustic power reduction $10\lg(St_h) + 10$ [dB]	experimental Umax ~ 60 m/s
10	Sinusoidal 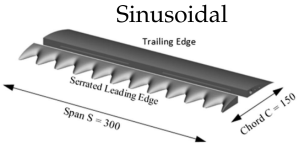 [20]	Biedermann et al. [20], 2017		☒	☒		Optimum as a function of turbulence parameters; low λ for low Tu	experimental Re ~ 10^5 (U ~ 61.4 m/s)
11	Various height slots 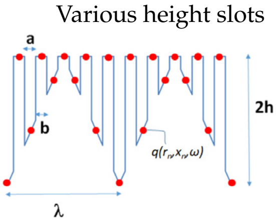 [43]	Chaitanya [43], 2017	☒		☒		Improved performance for f·(2 h)/U < 1	experimental Umax ~ 60 m/s
12	Sinusoidal 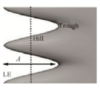 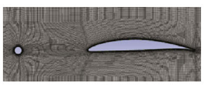 [45]	Tong et al. [45], 2018		☒		☒	Lower arodynamic fluctuations due to wavy LE; no directivity impact	numerical Umax ~ 40 m/s Re_{flow} ~ 4×10^5 Re_{rod} ~ 2.6×10^4
13	Sinusoidal 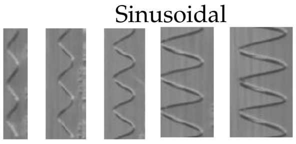 [16]	Narayanan et al. [16], 2015	☒		☒		Important noise reductions in the 1 < f·c/U < 3 range; similar for f > U/4 h	experimental Umax ~ 80 m/s

Table 1. *Cont.*

Crt. No.	Serration Shape	Author, Year	Solution Type		Type of Turbulence		Results	Observations
			2D	3D	Grid	Rod		
14	Sinusoidal 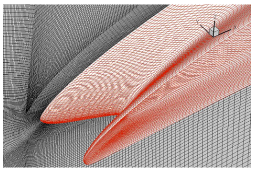 [14]	Clair et al. [14], 2012		☒			No lateral gust component can overestimate acoustic performance (below 3 kHz)	numerical; V.K. synthetic turbulence; Umax ~ 60 m/s
15	 [35]	Teruna et al. [35], 2020		☒		☒	Adding porous material to LE further increased the serration effects	numerical; M = 0.22; Re_{rod} ~ 4.8×10^4
16	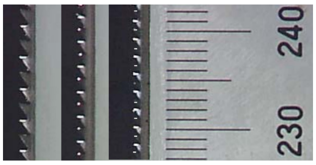 [46]	S. ITO [46], 2009		☒			Increased AoA range at low speeds; less violent laminar–turbulent transitions; low-intensity vorticies	experimental; no grid wind tunnel; Re ~ 5.5×10^5
17	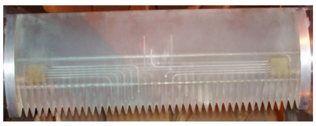 [23]	Polacsek et al. [23], 2011					Amiet's theory cannot fully reproduce experiments, but the numerical approach is close	experimental and numerical; synthetic turbulence; Umax ~ 60 m/s
18	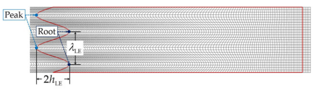 [19]	Kim et al. [19]		☒			OASPL decreases linearly with h; increasing profile thickness alters noise reduction	numerical; synthetic turbulence; Umax ~ 80 m/s
19	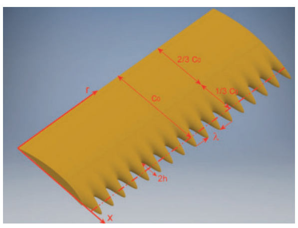 [47]	Lacagnina [47], 2021		☒			LE serations on 1/3 chord length; self-noise reduced by 3 dB; high λ—good in the mid-frequency area; low λ for less altered C_L	Experimental, Re ~ 4×10^5, Umax ~ 40 m/s

☒—checkmark for the type of solution and turbulence generation method identified in the cited paper.

Regarding the proposed modifications to the trailing edge, Table 2 highlights some of the relevant solutions identified in the literature.

Table 2. Modified blades on the trailing edge.

Crt. No.	Serration Shape	Author, Year	Solution Type 2D	Solution Type 3D	Results/Observations
1	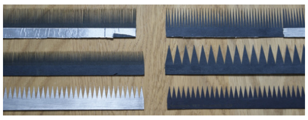 [40]	Gruber [40], 2012	☒		Experimental; Umax ~ 80 m/s Noise increases at high frequencies, contrary to theory. Acoustic power reduction increases with decreasing λ/δ; in the high frequency range, OASPL is proportional to f^{-5}
	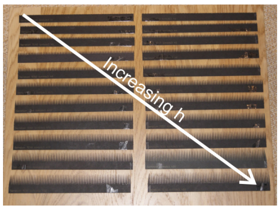 [40]				
	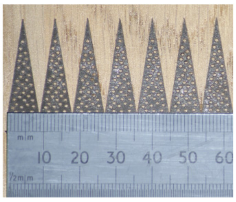 [40]		☒		Performance depends very little on incidence (porosity 8–10%); poorer performance than the non-perforated version (at medium frequencies)
	 [40]				
	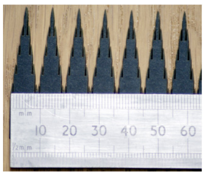 [40]		☒		The reduction increases with increasing channel depth (at f > 500 Hz); the effect is maintained even at high f, up to 10 kHz; a smaller channel width is desirable Umax ~ 80 m/s
	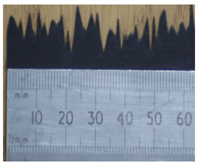 [40]		☒		Lower amplitude tends to achieve a better and more consistent reduction over a wider frequency band Umax ~ 80 m/s
2	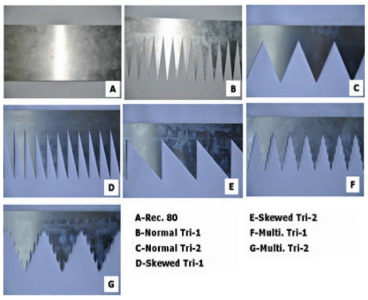 [34]	Ryi & Choi [34], 2018	☒		Variants with λ/h = 2 perform better at low frequencies ~1 kHz (compared to λ/h = 1); aerodynamically, the same trend was identified (higher C_L for high λ) Experimental Umax ~ 30 m/s

Table 2. *Cont.*

Crt. No.	Serration Shape	Author, Year	Solution Type 2D	Solution Type 3D	Results/Observations	
3	Triangular serrations	Lyu et al. [28], 2015	☒		$\omega h/U >> 1$ (Howe) = kc > 1; kh >> 1 for good performance; Higher ΔOASLP with increasing h/λ ratios; Very high h/λ ~ good at high f.	Analytical, imposed turbulence, M = 0.1
4	 [27]	Moreau et al. [27], 2012	☒		$St_\delta = 1$ delimits noise reduction/increase zones; Narrow serrations: $St_\delta < 0.13$; Wide serrations: $St_\delta < 0.2$	Experimental Umax ~ 38 m/s Re ~ (2–8.3) × 10^5
5	Triangular serrations	Howe [25], 1991	☒		Noise reduction law: $10\lg(1 + (2 \cdot 2h/\lambda)^2)$ [dB] for $\lambda/h < 4$	Analythical
6	 [31]	Liu et al. [31], 2015		☒	The PSD spectrum decreases in intensity near the serration root; Serrations do not modify the CZ = f(α) shape but lower the value	Experimental Umax ~ 50 m/s Re ~ (2–2.5) × 10^5
7	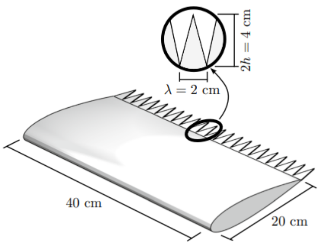 [32]	Leon et al. [32], 2016		☒	Acoustic power depends on the flow deflection angle obtained by the serration $\Psi \approx \Psi_0 \sin^2(\theta_0 + \gamma)$	Umax ~ 45 m/s
8	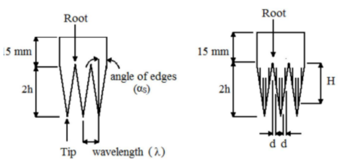 [48]	Liu et al. [48], 2016		☒	At high incidents, turbulent areas with high PSD move from above the chord line to below it	Experimental Umax ~ 60 m/s Re ~ 3 × 10^5
9	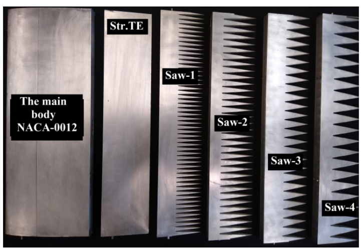 [26]	Al Tlua [26], 2021		☒	Triangular serrations reduce overall noise but add tonal components (which depend on U, 2h, λ, profile thickness, and background noise)	Experimental and numerical; Umax ~ 24 m/s Re ~ 5 × 10^5

Table 2. *Cont.*

Crt. No.	Serration Shape	Author, Year	Solution Type		Results/Observations	
			2D	3D		
10	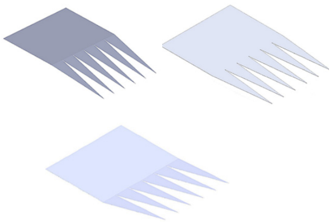 [26]	Woodhead et al. [26], 2021	☒		When oriented downward, the serrations lose efficiency over the whole frequency range. Facing upwards, 3 areas of interest are distinguished: low-perf low frequencies; medium frequencies-redistribution of turbulent; and rising performance areas	Experimental and numerical; Umax ~ 24 m/s Re ~ 2.96 × 10^5
11	 [49] 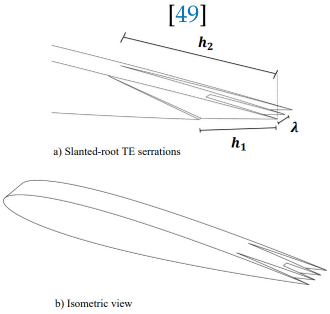 [49]	Salama [49], 2021	☒		Synthetic turbulence ("Vortex Method"); RANS and LES simulations; At low AoA, below 1 dB noise reduction in the range 200–10,000 Hz (experimentally confirmed)	Experimental and numerical; Umax ~ 24 m/s Re ~ 5 × 10^5

☒—checkmark for the type of solution identified in the cited paper.

Combined serrations or configurations different from those in Tables 1 and 2 are shown in Table 3.

Table 3. Special configurations for serrated blades.

Crt. No.	Serration Shape	Author, Year	Solution Type		Results/Observations
			2D	3D	
1	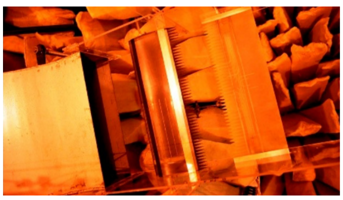 [40]	Gruber [40], 2012		☒	Experimental; Umax ~ 80 m/s; LE + TE (tandem) serrations; OAPWL decreases with decreasing Λ/λ (especially for Λ/λ < 0.3); optimal LE shape λ ≥ 3Λ

Table 3. *Cont.*

Crt. No.	Serration Shape	Author, Year	Solution Type		Results/Observations
			2D	3D	
2	 [50]	Alimeri et al. [50], 2015		☒	Experimental and numerical; Re ~ 10^5 The stator pressure loss coefficient is better over the entire range of −37°–10° using wavy surface vanes
3	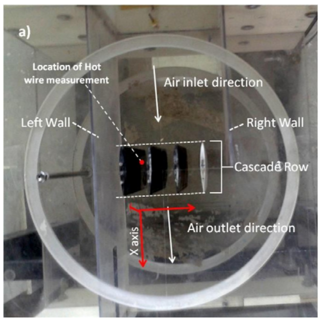 [51]	Rajeshwaran & Kushari [51], 2015		☒	Experimental, Umax ~ 35 m/s; LE serrations; cascade, flow visualization with oleic acid and titanium dioxide; lowest velocity is behind the serration root; pressure losses are proportional to the frontal area of the vane; flow separation point moves backwards so that overall the vane delays the occurrence of stall compared to the reference
4	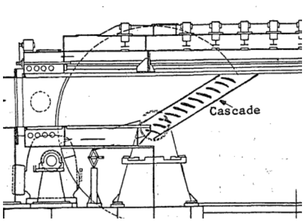 [52]	Smith & Sowers [52], 1974		☒	Experimental, Umax ~ 0.87; LE serrations; configuration with 2 or 6 vanes in cascade; vanes with c = 5 cm; serration amplitude must be above 6%·c; 2h/λ < 1.5; improvements on both flow and noise
5	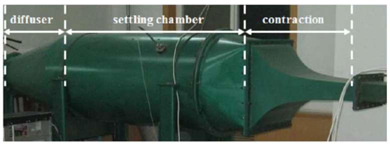 [53]	Qiao et al. [53], 2014		☒	Experimental, Re ~ 5 × 10^5; Umax ~ 50 m/s TE serrations; λ/h = 0.5 much better than λ/h = 1; the range of frequencies in which noise reduction is achieved widens as fluid velocity increases
6	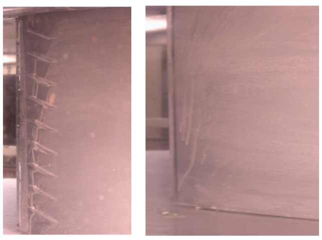 [54]	Craig [54], 2005		☒	Experimental, Re ~ 3.8 × 10^5, Umax ~ 25 m/s; cascade; slots at LE and TE through which air is blown; tonal component of interest reduced by more than 20 dB in some combinations; unstable separations at too low or too high flow rates; an optimum was identified at a 2.5% blown flow rate

Table 3. *Cont.*

Crt. No.	Serration Shape	Author, Year	Solution Type		Results/Observations
			2D	3D	
7	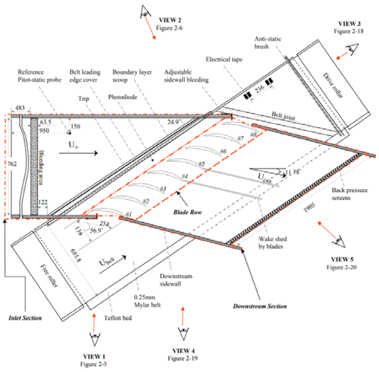 [55]	Geiger [55], 2004		☒	Experimental, Re ~ 3.9×10^5, Umax ~ 25 m/s; TE serrations; cascade; periodic aerodynamic spanwise behavior; smaller amplitudes were found to perform better (better blade loading, less turbulent structures)
8	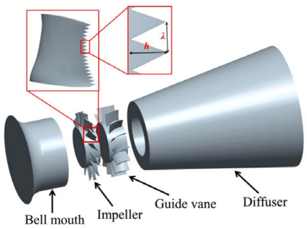 [56]	Ye et al. [56], 2022		☒	Numerical, Δp* = 2244 Pa, Q = 37.1 m^3/s; serrated rotor; noise reduction in the low frequency area; in the area of interest, the reduction is 6.7 dB with over 20 dB reduction in the tonal component; the serrations break up the large swirls into smaller formations that dissipate better
9	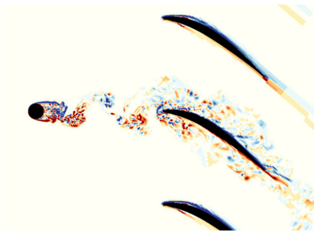 [57]	Teruna et al. [57], 2019		☒	Numerical, Umax ~ 75 m/s; rod–cascade configuration; the rod can impact the flow similar to what a real stator stage experiences; greater reductions can be achieved by "treating" the aerodynamic surface
10	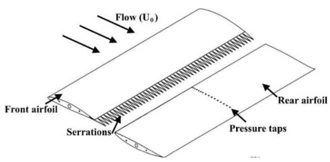 [47]	Liu et al. [47], 2019	☒		Experimental setup: maximum flow velocity approximately Umax ~ 30 m/s; trailing edge (TE) serrations implemented; configured in tandem; observed noise reductions exceeding 9 dB at frequencies below 1.5 kHz; rapid decay of turbulent structures
11	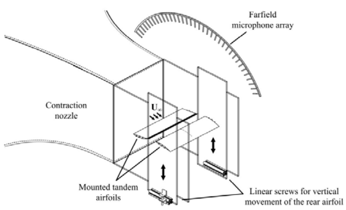 [58]	Liu et al. [58], 2021			Experimental, Umax ~ 30 m/s; TE serrations; tandem configuration; sharper blades behaved better; pressure fluctuations recorded on the blade show that the first 30% of the chord length determines the blade loading (very easily influenced by the forward blade wake)

Table 3. *Cont.*

Crt. No.	Serration Shape	Author, Year	Solution Type		Results/Observations
			2D	3D	
12	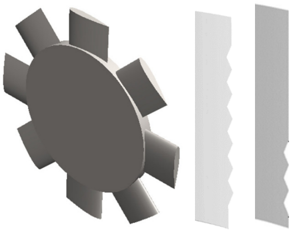 [59]	Alkhalifa et al. [59], 2022		☒	Numerical, Wells turbine; full or partial serration; better behavior of a partially serrated blade (efficiency)
13	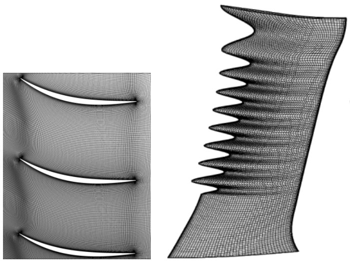 [60]	Polacsek et al. [60], 2022			Numerical, Umax ~ 120(..193)m/s; 2 h/c limit is 0.15; 4–6 dB reduction based on empirical observations on the variation in serration parameters

☒—checkmark for the type of solution identified in the cited paper.

As special configurations identified in the literature, there are also vanes with dimples on the suction side [24,61] or finlets [61] either on the leading or trailing edge. Blowing or suction in specific areas of the blade (close to the leading edge or at the root of the serration) looks promising [62]. Similar to finlets, Zhang et al. [63] approached the solution both numerically and experimentally, with ridges placed at both the leading and trailing edges. At low incident and flow speeds, they tend to reduce OASPL even up to 20 dB. The behavior of a serrated blade with ports at the leading edge has been identified as having interesting (in some cases, very good) aerodynamic performance, with Al-Okbi [44] testing such a geometry at different angles of attack. Amirsalari [64] also identified in the literature geometries featuring porous inserts (such as flat plate types) that, when placed at or downstream of the leading edge, mitigate low-frequency noise without increasing high-frequency noise. The use of cylindrical finlets of different lengths has been addressed by Fiscaletti [65], showing, in addition to noise control, aerodynamic improvements such as a 12% reduction in drag coefficient. Obviously, some combinations of incident and size led to noise increases by increasing the high-frequency components.

5. Discussions

It can be seen that several methods have been identified for shaping the acoustic radiation emitted by a vane whose leading or trailing edge has been modified. At present, the most common modifications are the placement of periodic structures, called serations, with a cutout appearance, which, with a judicious choice of the defining parameters in relation to the operating conditions, can lead to much improved acoustic performance. The placement of special materials (porous or metamaterials) in key areas has been identified as a good solution from an acoustic point of view, but aerodynamic implications must also be taken into account. As presented, there are numerous solutions, both applied to the leading edge and the trailing edge. Combined solutions are less used, which could be a starting point for future research. The conclusions drawn from the various authors cited throughout the paper suggest that a combined solution may be more efficient than an isolated one.

It should also be noted that solutions applied to an isolated blade may yield favorable results, but when applied to a cascade, their behavior may be altered in this configuration. Fortunately, there is research on the behavior of serrated blade cascades that supports the notion that noise reduction can be achieved under such conditions.

Author Contributions: Conceptualization, A.-G.T. and G.C.; methodology, A.-G.T.; validation, D.-E.C.; investigation, G.C. and A.-G.T.; data curation, A.-G.T.; writing—original draft preparation, A.-G.T., G.C. and D.-E.C.; writing—review and editing, A.-G.T., G.C. and D.-E.C. All authors have read and agreed to the published version of the manuscript.

Funding: This research received no external funding.

Data Availability Statement: No new data were created.

Conflicts of Interest: The authors declare no conflicts of interest.

Nomenclature

a_0	speed of sound [m/s]
c	chord length [m]
e	airfoil maximum thickness [m]
f	frequency [Hz]
h (or 2 h)	serration amplitude
h/δ	the dimensionless parameter of the serration amplitude [-]
h/λ	the dimensionless parameter associated with the serration angle [-]
k	wave number [m^{-1}]
M	Mach number [-]
L	airfoil length [m]
Re	Reynolds number [-]
St_δ	Strouhal number [-]
U_0	(averaged) speed of the jet [m/s]
U_c	convection speed [m/s]
δ	turbulent boundary layer thickness [m]
λ	serration pitch [m]
θ	observer angle [°]
ω	angular frequency [rad/Hz]
$\omega\delta/U_c$	dimensionless frequency parameter [-]
Λ	turbulence integral length scale [m]
BPF	blade passing frequency [Hz]
PSD	power spectal density [W/Hz]
SPL	sound pressure level [dB]
OASPL	overall sound pressure level [dB]

Other notations and abbreviations were defined throughout the paper.

References

1. Document 02002L0049-20210729, DIRECTIVE 2002/49/EC of the European Parliament and of the Council of 25 June 2002 Relating to the Assessment and Management of Environmental Noise. 2002. Available online: https://eur-lex.europa.eu/legal-content/EN/TXT/?uri=CELEX:02002L0049-20210729 (accessed on 16 February 2024).
2. Law No. 121 on the Assessment and Management of Ambient Noise, Romanian Parliament, Romania, 3 July 2019. Available online: https://www.caa.ro/w.htm/pages/legislatie-mediu (accessed on 16 February 2024).
3. Document 32008R0216, Regulation (EC) No 216/2008 of the European Parliament and of the Council of 20 February 2008 on Common Rules in the Field of Civil Aviation and Establishing a European Aviation Safety Agency, and Repealing Council Directive 91/670/EEC, Regulation (EC) No 1592/2002 and Directive 2004/36/EC (Text with EEA Relevance), OJ L 79, 19.03.2008. Available online: https://eur-lex.europa.eu/legal-content/EN/TXT/?qid=1474978980580&uri=CELEX:32008R0216 (accessed on 16 February 2024).
4. Document 32012R0748, Commission Regulation (EU) No 748/2012 of 3 August 2012 Laying down Implementing Rules for the Airworthiness and Environmental Certification of Aircraft and Related Products, Parts and Appliances, as well as for the Certification of Design and Production Organisations (Recast) Text with EEA Relevance, OJ L 224, 21.8.2012, pp. 1–85. Available online: https://eur-lex.europa.eu/legal-content/EN/TXT/?qid=1473415871666&uri=CELEX:32012R0748 (accessed on 16 February 2024).
5. Document 32014R0598, Regulation (EU) No 598/2014 of the European Parliament and of the Council of 16 April 2014 on the Establishment of Rules and Procedures with Regard to the Introduction of Noise-Related Operating Restrictions at Union Airports within a Balanced Approach and Repealing Directive 2002/30/EC, OJ L 173, 12.6.2014, pp. 65–78. Available online: https://eur-lex.europa.eu/legal-content/EN/TXT/?uri=celex:32014R0598 (accessed on 16 February 2024).

6. Document 32006L0093, Directive 2006/93/EC of the European Parliament and of the Council of 12 December 2006 on the Regulation of the Operation of Aeroplanes Covered by Part II, Chapter 3 , Volume 1 of Annex 16 to the Convention on International Civil Aviation, Second Edition (1988) (Codified Version) (Text with EEA Relevance), OJ L 374, 27.12.2006, pp. 1–4. Available online: https://eur-lex.europa.eu/legal-content/EN/TXT/?uri=CELEX:32006L0093 (accessed on 16 February 2024).
7. Curle, N. The influence of solid boundaries upon aerodynamic sound. *Proc. R. Soc. London. Ser. A. Math. Phys. Sci.* **1955**, *231*, 505–514. [CrossRef]
8. Turner, J.M.; Kim, J.W. Quadrupole noise generated from a low-speed aerofoil in near- and full-stall conditions. *J. Fluid Mech.* **2022**, *936*, A34. [CrossRef]
9. Lighthill, M.J. On Sound Generated Aerodynamically. I. General Theory. *Proc. R. Soc. London. Ser. A Math. Phys. Sci.* **1952**, *211*, 564–587.
10. Amiet, R. Acoustic radiation from an airfoil in a turbulent stream. *J. Sound Vib.* **1975**, *41*, 407–420. [CrossRef]
11. Tian, Y.; Cotté, B.; Chaigne, A. Wind Turbine Noise Modelling Based on Amiet's Theory. In Proceedings of the 5th International Meeting on Wind Turbine Noise, Denver, CO, USA, 28–30 August 2013.
12. Lyu, B.; Azarpeyvand, M. On the noise prediction for serrated leading edges. *J. Fluid Mech.* **2017**, *826*, 205–234. [CrossRef]
13. Weger, M.; Wagner, H. Morphological Variations of Leading-Edge Serrations in Owls (Strigiformes). *PLoS ONE* **2016**, *11*, e0149236. [CrossRef] [PubMed]
14. Clair, V.; Polacsek, C.; Le Garrec, T.; Reboul, G. CAA methodology to simulate turbulence-airfoil noise. In Proceedings of the 18th AIAA/CEAS Aeroacoustics Conference (33rd AIAA Aeroacoustics Conference), Colorado Springs, CO, USA, 4–6 June 2012. [CrossRef]
15. Lau, A.S.; Haeri, S.; Kim, J.W. The effect of wavy leading edges on aerofoil–gust interaction noise. *J. Sound Vib.* **2013**, *332*, 6234–6253. [CrossRef]
16. Narayanan, S. *Airfoil Noise Reductions through Leading Edge Serrations*; University of Southampton: Southampton, UK.
17. Narayanan, S.; Joseph, P.; Haeri, S.; Kim, J.; Paruchuri, C.; Polacsek, C. Noise Reduction Studies from the Leading Edge of Serrated Flat Plates. In Proceedings of the 20th AIAA/CEAS Aeroacoustics Conference, Atlanta, GA, USA, 16–20 June 2014.
18. Paruchuri, C.C.; Narayanan, S.; Joseph, P.; Kim, J.W. Leading edge serration geometries for significantly enhanced leading edge noise reductions. In Proceedings of the 22nd AIAA/CEAS Aeroacoustics Conference, Lyon, France, 30 May–1 June 2016. [CrossRef]
19. Kim, J.W.; Haeri, S.; Joseph, P.F. On the reduction of aerofoil–turbulence interaction noise associated with wavy leading edges. *J. Fluid Mech.* **2016**, *792*, 526–552. [CrossRef]
20. Biedermann, T.M.; Chong, T.P.; Kameier, F.; Paschereit, C.O. Airfoil Noise Subjected to Leading-Edge Serrations. *AIAA J.* **2017**, *55*, 3128–3142. [CrossRef]
21. Amiet, R. Airfoil gust response and the sound produced by airfoil-vortex interaction. *J. Sound Vib.* **1986**, *107*, 487–506. [CrossRef]
22. Paterson, W.; Amiet, R.K. Acoustic Radiation and Surface Pressure Response of an Airfoil Due to Incident Turbulence. NASA CR-2733. Available online: https://ntrs.nasa.gov/citations/19760025886 (accessed on 16 February 2024).
23. Polacsek, C.; Clair, V.; Reboul, G.; Denia, H. *Turbulence-Airfoil Interaction Noise Reduction Using Wavy Leading Edge: An Experimental and Numerical Study*; Institute of Noise Control Engineering/Japan & Acoustical Society of Japan: Osaka, Japan, 2011; pp. 170–180.
24. Buszyk, M.; Polacsek, C.; Le Garrec, T.; Barrier, R.; Clair, V.; Salze, E.; Bailly, C. Aeroacoustic assessment of a rectilinear cascade with leading edge serrations: Predictions and measurements. *Comput. Fluids* **2024**, *271*, 106179. [CrossRef]
25. Howe, M.S. Noise Produced by a Sawtooth Trailing Edge. *J. Acoust. Soc. Am.* **1991**, *90*, 482. [CrossRef]
26. Al Tlua, B. Experimental Wind Tunnel Testing and Numerical Optimization Studies for Airfoil Trailing Edge Noise Reduction. Ph.D. Thesis, Ottawa-Carleton Institute for Mechanical and Aerospace Engineering, Ottawa, ON, Canada, 2021.
27. Moreau, D.; Brooks, L.; Doolan, C. On the noise reduction mechanism of a flat plate serrated trailing edge at low-to-moderate Reynolds number. In Proceedings of the 18th AIAA/CEAS Aeroacoustics Conference (33rd AIAA Aeroacoustics Conference), Colorado Springs, CO, USA, 4–6 June 2012.
28. Lyu, B.; Azarpeyvand, M.; Sinayoko, S. Prediction of noise from serrated trailingedges. *J. Fluid Mech.* **2016**, *793*, 168. [CrossRef]
29. Lau, A.S.H.; Huang, X. The control of aerodynamic sound due to boundary layer pressure gust scattering by trailing edge serrations. *J. Sound Vib.* **2018**, *432*, 133–154. [CrossRef]
30. Woodhead, P.C.; Chong, T.P.; Joseph, P.F.; Vathylakis, A. Aerofoil self-noise radiations subjected to serration flap angles. *Exp. Fluids* **2021**, *62*, 152. [CrossRef]
31. Liu, X.; Azarpeyvand, M.; Theunissen, R. Aerodynamic and Aeroacoustic Performance of Serrated Airfoils. In Proceedings of the 21st AIAA/CEAS Aeroacoustics Conference, Dallas, TX, USA, 22–26 June 2015. [CrossRef]
32. León, C.A.; Ragni, D.; Pröbsting, S.; Scarano, F.; Madsen, J. Flow topology and acoustic emissions of trailing edge serrations at incidence. *Exp. Fluids* **2016**, *57*, 1–17. [CrossRef]
33. Chen, W.; Mao, L.; Xiang, K.; Tong, F.; Qiao, W. The Application of a Linear Microphone Array in the Quantitative Evaluation of the Blade Trailing-Edge Noise Reduction. *Appl. Sci.* **2021**, *11*, 57. [CrossRef]
34. Ryi, J.; Choi, J. Estimation Method to Achieve a Noise Reduction Effect of Airfoil with a Serrated Trailing Edge for Wind Turbine Rotor. In *Stability Control and Reliable Performance of Wind Turbines*; InTech: Rijeka, Italy, 2018. [CrossRef]
35. Teruna, C.; Avallone, F.; Casalino, D.; Ragni, D. Numerical investigation of leading edge noise reduction on a rod-airfoil configuration using porous materials and serrations. *J. Sound Vib.* **2020**, *494*, 115880. [CrossRef]

36. Jiang, M.; Li, X.-D.; Zhou, J.-J. Experimental and numerical investigation on sound generation from airfoil-flow interaction. *Appl. Math. Mech.* **2011**, *32*, 765–776. [CrossRef]
37. Greschner, B.; Peth, S.; Moon, Y.J.; Seo, J.H.; Jacob, M.C.; Thiele, F. Three-dimensional predictions of the rod wake-airfoil interaction noise by hybrid methods. In Proceedings of the 14th International Congress on Sound and Vibration 2007, ICSV 2007, Cairns, Australia, 9–12 July 2007; Volume 2, pp. 1599–1610.
38. Sreenivasan, A.A.R.; Iyer, B.K. Enhanced wall turbulence model for flow over cylinder at high Reynolds number. *AIP Adv.* **2019**, *9*, 095012. [CrossRef]
39. Liu, L.; Zhang, L.; Wu, B.; Chen, B.; Aecom, P. Numerical and Experimental Studies on Grid-Generated Turbulence in Wind Tunnel. *J. Eng. Sci. Technol. Rev.* **2017**, *10*, 159–169. [CrossRef]
40. Gruber, M. Airfoil Noise Reduction by Edge Treatments. Ph.D. Thesis, University of Southampton, Southampton, UK, 2012. Available online: https://eprints.soton.ac.uk/349012/ (accessed on 16 February 2024).
41. Chaitanya, P.; Joseph, P.; Narayanan, S.; Vanderwel, C.; Turner, J.; Kim, J.W.; Ganapathisubramani, B. Performance and mechanism of sinusoidal leading edge serrations for the reduction of turbulence–aerofoil interaction noise. *J. Fluid Mech.* **2017**, *818*, 435–464. [CrossRef]
42. Lyu, B.; Ayton, L.J. Rapid noise prediction models for serrated leading and trailing edges. *J. Sound Vib.* **2019**, *469*, 115136. [CrossRef]
43. Paruchuri, C. Aerofoil Geometry Effects on Turbulence Interaction Noise. Ph.D. Thesis, University of Southampton, Southampton, UK, 2017. Available online: https://eprints.soton.ac.uk/415884/ (accessed on 16 February 2024).
44. Al-Okbi, Y.; Chong, T.P.; Stalnov, O. Leading Edge Blowing to Mimic and Enhance the Serration Effects for Aerofoil. *Appl. Sci.* **2021**, *11*, 2593. [CrossRef]
45. Tong, F.; Qiao, W.; Chen, W.; Cheng, H.; Wei, R.; Wang, X. Numerical analysis of broadband noise reduction with wavy leading edge. *Chin. J. Aeronaut.* **2018**, *31*, 1489–1505. [CrossRef]
46. Ito, S. Aerodynamic Influence of Leading-Edge Serrations on an Airfoil in a Low Reynolds Number—A Study of an Owl Wing with Leading Edge Serrations. *J. Biomech. Sci. Eng.* **2009**, *4*, 117–123. [CrossRef]
47. Lacagnina, G.; Chaitanya, P.; Kim, J.-H.; Berk, T.; Joseph, P.; Choi, K.-S.; Ganapathisubramani, B.; Hasheminejad, S.M.; Chong, T.P.; Stalnov, O.; et al. Leading edge serrations for the reduction of aerofoil self-noise at low angle of attack, pre-stall and post-stall conditions. *Int. J. Aeroacoustics* **2020**, *20*, 130–156. [CrossRef]
48. Liu, X.; Jawahar, H.K.; Azarpeyvand, M.; Theunissen, R. Wake Development of Airfoils with Serrated Trailing Edges. In Proceedings of the 22nd AIAA CEAS Aeroacoustics Conference [AIAA 2016-2817] American Institute of Aeronautics and Astronautics Inc. (AIAA), Lyon, France, 30 May–1 June 2016.
49. Salama, Y. Experimental and Numerical Investigation of Bio-Inspired Airfoil Trailing-Edge Designs for Noise Reduction. Available online: https://repository.library.carleton.ca/concern/etds/k06988420 (accessed on 16 February 2024).
50. Shyam, V.; Ameri, A.; Poinsatte, P.; Thurman, D.; Wroblewski, A.; Snyder, C. Application of Pinniped Vibrissae to Aeropropulsion. In Proceedings of the ASME Turbo Expo 2015: Turbine Technical Conference and Exposition, Montreal, QC, Canada, 15–19 June 2015. [CrossRef]
51. Rajeshwaran, M.S.; Kushari, A. Experimental Study on the Flow Past Sinusoidal Leading Edge Serrations in a Compressor Cascade. In Proceedings of the ASME 2015 Gas Turbine India Conference, Hyderabad, India, 2–3 December 2015. [CrossRef]
52. Smith, E.G.; Sowers, H.D. Cascade Tests of Serrated Leading Edge Blading at High Subsonic Speeds. NASA CR-2472; 1974. Available online: https://ntrs.nasa.gov/api/citations/19750003911/downloads/19750003911.pdf (accessed on 16 February 2024).
53. Qiao, W.; Ji, L.; Tong, W.; Xu, K.; Chen, W. Application of Phased Array în the Study of Linear Cascade Noise Reduction on the Indoor Test Bed. In Proceedings of the 5th Berlin Beamforming Conference, Berlin, Germany, 19–20 February 2014.
54. Craig, M.E. Trailing-Edge Blowing of Model Fan Blades for Wake Management. Master's Thesis, Virginia Polytechnic Institute and State University, Blacksburg, VA, USA, 2005. Available online: https://vtechworks.lib.vt.edu/server/api/core/bitstreams/047d5593-a779-47d8-86a4-ee7ca22a75aa/content (accessed on 16 February 2024).
55. Geiger, D. Comparative Analysis of Serrated Trailing Edge Designs on Idealized Aircraft Engine Fan Blades for Noise Reduction. Master's Thesis, Virginia Polytechnic Institute and State University, Blacksburg, VA, USA, 2004. Available online: https://vtechworks.lib.vt.edu/items/6caef5e2-88ac-4037-b95c-7f5bfa4fbc51 (accessed on 16 February 2024).
56. Ye, X.; Zheng, N.; Zhang, R.; Li, C. Effect of serrated trailing-edge blades on aerodynamic noise of an axial fan. *J. Mech. Sci. Technol.* **2022**, *36*, 2937–2948. [CrossRef]
57. Teruna, C.; Ragni, D.; Avallone, F.; Casalino, D. A rod-linear cascade model for emulating rotor-stator interaction noise in turbofans: A numerical study. *Aerosp. Sci. Technol.* **2019**, *90*, 275–288. [CrossRef]
58. Liu, X.; Zang, B.; Azarpeyvand, M. Wake-aerofoil interaction noise control with trailing-edge serrations. *Exp. Therm. Fluid Sci.* **2021**, *130*, 110510. [CrossRef]
59. Alkhalifa, A.S.; Uddin, M.N.; Atkinson, M. Aerodynamic Performance Analysis of Trailing Edge Serrations on a Wells Turbine. *Energies* **2022**, *15*, 9075. [CrossRef]
60. Polacsek, C.; Cader, A.; Buszyk, M.; Barrier, R.; Gea-Aguilera, F.; Posson, H. Aeroacoustic design and broadband noise predictions of a fan stage with serrated outlet guide vanes. *Phys. Fluids* **2020**, *32*, 107107. [CrossRef]

61. Kumar, S.; Singh, S.K.; Jha, S.; Baskaran, K.; Srinivasan, K.; Narayanan, S. On the reductions of airfoil broadband noise through circular dimples. *Appl. Acoust.* **2024**, *217*, 109819. [CrossRef]
62. Yang, C.; Liu, Y.; Zhang, X.; Bi, C. Hybrid control of aerofoil self-noise by coupling air blowing and trailing-edge serration. *J. Sound Vib.* **2024**, *575*, 118265. [CrossRef]
63. Zhang, C.; Cheng, W.; Du, T.; Sun, X.; Shen, C.; Chen, Z.; Liang, D. Experimental and numerical study on noise reduction of airfoil with the bioinspired ridge-like structure. *Appl. Acoust.* **2023**, *203*, 109190. [CrossRef]
64. Amirsalari, B.; Rocha, J. Recent Advances in Airfoil Self-Noise Passive Reduction. *Aerospace* **2023**, *10*, 791. [CrossRef]
65. Fiscaletti, D.; Pereira, L.T.L.; Ragni, D. Finlet rails for the reduction of the trailing-edge noise. *J. Sound Vib.* **2024**, *568*, 118072. [CrossRef]